energies

MDPI

Article

Analysis of Integration of MEA-Based CO_2 Capture and Solar Energy System for Coal-Based Power Plants Based on Thermo-Economic Structural Theory

Rongrong Zhai [1,*], Hongtao Liu [1], Hao Wu [1], Hai Yu [2] and Yongping Yang [1]

[1] School of Energy Power and Mechanical Engineering, North China Electric Power University, Beijing 102206, China; liuhongtao183@gmail.com (H.L.); ncepuwh@163.com (H.W.); ncepuyyp@163.com (Y.Y.)
[2] CSIRO Energy, 10 Murray Dwyer Circuit, Mayfield West, NSW 2304, Australia; hai.yu@csiro.au
* Correspondence: zhairongrong01@163.com; Tel./Fax: +86-10-6177-2284

Received: 21 March 2018; Accepted: 10 May 2018; Published: 17 May 2018

Abstract: Installing CO_2 capture plants in coal-fired power stations will reduce greenhouse gas emissions and help mitigate climate change. However, the deployment of this technology faces many obstacles—in particular, high energy consumption. Aiming to address this challenge, we investigated the integration of a solar energy system in a 1000 MW coal-fired power plant equipped with monoethanolamine (MEA)-based CO_2 capture (termed PG-CC) by comparing the thermo-economic performance of two integrated systems with that of PG-CC. In the first system, solar-aided coal-fired power generation equipped with MEA-based CO_2 capture (SA-PG-CC), solar thermal was used to heat the high-pressure feed water in the power plant, while the reboiler duty of the capture plant's stripper was provided by extracted low-pressure steam from the power plant. The second system integrated the power plant with solar-aided MEA-based CO_2 capture (SA-CC-PG), using solar thermal to heat the stripper's reboiler. Both systems were simulated in EBSILON Professional and Aspen Plus and analysed using thermo-economics theory. We then evaluated each system's thermodynamic and economic performance in terms of power generation and CO_2 capture. Compared with PG-CC, the thermo-economic cost of electricity increased by 12.71% in SA-PG-CC and decreased by 9.77% in SA-CC-PG. The unit thermo-economic cost of CO_2 was similar in both the PG-CC and SA-PG-CC systems, but significantly greater in SA-CC-PG. Overall, SA-PG-CC produced less power but used energy more effectively than SA-CC-PG. From a thermo-economic point of view, SA-PG-CC is therefore a better choice than SA-CC-PG.

Keywords: MEA-based CO_2 capture; solar energy system; coal-fired power generation; thermo-economic theory

1. Introduction

Human society and the ecological environment are facing enormous challenges due to the significant increase in greenhouse gas emissions and consequent climate change [1,2]. Thermal power-plant emissions make up more than 40% of global CO_2 emissions, 70% of which are produced by coal-fired power plants [3]. Installing CO_2 capture and storage in thermal power plants—especially coal-fired power plants—is therefore one of the most direct and effective measures to reduce CO_2 emissions and help mitigate global warming [4].

Post-combustion carbon capture is the most feasible end-of-pipe technology for the large fleet of existing coal-fired power stations. Chemical absorption-based capture has been commercially realised in some coal-fired power stations, including the Boundary Dam and WA Parish power plants [5,6]. The basic principal of the technique is to absorb CO_2 through chemical reaction with absorbents at

low temperatures in the absorber, and then regenerate CO_2 at high temperatures in the stripper [7,8]. Monoethanolamine (MEA)-based CO_2 capture is the most-studied system. It has a relatively high CO_2 loading capacity and a high absorption rate [9], but these advantages are outweighed by the high energy requirement for MEA regeneration [10,11].

Efforts to reduce the energy penalty on the power generation with post-combustion carbon capture generally fall into three main categories: (i) improvements to the CO_2 capture process through use of better solvents, improved solvent formulations and process intensification [12–27], (ii) energy recovery during CO_2 integration with power plants [28–37], and (iii) integration with renewable energy sources, such as solar energy system [23–27].

Within the first category, efforts have been mainly focused on development of better solvents and capture process improvement, intensification and optimisation. Currently, more than 10 companies/organisations can provide near-term solvent-based capture technologies for CO_2 capture in coal-fired power stations, and these technology suppliers include Shell Cansolv, MHI, Fluor, BASF, Siemens, and University of Texas at Austin [12]. The improved solvents are mainly based on chemicals that possess amino functional groups, such as aqueous ammonia, amino acid salts and amines. For example, MHI developed the KS-1 solvent, which is based on sterically hindered amine solvent, and the company claimed that the solvent regeneration energy is 68% that of the MEA-based process and solvent loss and degradation are 10% of MEA [13]. The technology has recently been applied in a commercial project—Petra Nova Carbon Capture Project at W.A. Parish Power Plant in USA—to capture 1.4 million tonnes of CO_2 per annum [14]. It has also been found that an MEA concentration of 40 wt % has a lower energy demand than 30 wt % [15]. Apart from the solvent development, process improvement, intensification and optimisation can also improve the capture performance. Even for the MEA-based process, the minimum regeneration energy in the MEA process could fall to 3.1 MJ/kg CO_2 through combined parameter optimisation and process modification [16]. Simplification of vapour compression configuration can decrease energy consumption from 3.26 to 2.90 MJ/kg CO_2 [17]. Pilot plant trials at University of Texas at Austin have shown that with an advanced flash stripper, the capture process based on 5 m piperazine (mole/kg water) can achieve regeneration energies of 2.1–2.5 GJ/tonne CO_2 [18]. The process simulation showed that an advanced aqueous ammonia-based process that incorporates the combined flash stripping and a cold rich split can achieve a very competitive regeneration duty of 1.86 MJ/kg CO_2 at an optimised stripper pressure of 12 bar and an NH_3 concentration of 10.2 wt % [19]. In addition to the further development of near-term technologies, intensive research work has been carried out to develop novel solvents, including ionic liquids [20], enzyme catalysed solvents [21], and phase change solvents [22]. These novel solvents are still in the early stages of development. The location of steam extraction also effects the efficiency penalty. Extraction from the cross-over pipe between the IP and LP turbines and that from within the LP steam turbine can both reduce the efficiency penalty incurred by CO_2 capture [23]. Other process configurations that can decrease the energy penalty have been reviewed, including: a stripper operating with moderate vacuum pressure (around 0.75 bar), the staged feed of the stripper, multi-pressure stripping, lean solvent vapour compression, absorber intercooling, condensate heating, condensate evaporation, stripper overhead compression, lean amine flash, split-amine flow, rich split, multi-component columns, inter-stage temperature control, vapour recompression, and matrix stripping [24–27].

In the category of energy recovery, there are three approaches to recovery of waste energy: (a) heat recovery or heat integration within the power plant to improve efficiency; (b) waste heat recovery from the CO_2 capture process to use in the power plant and improve efficiency; (c) heat recovery from the power plant to use in the CO_2 capture process, reducing the energy penalty [28]. Harkin (2009) reviewed the consideration of heat integration in CO_2 capture coal-fired power stations and the integration of the brown coal dewatering processes into a power plant with CCS. The study showed a reduced energy penalty in the heat integration power plant and a higher energy-saving potential by pre-drying of the coal [29,30]. Xu et al. (2014) adopted three measures to recover the

surplus energy from the CO_2 capture process: (1) using a portion of low-pressure steam instead of high-pressure extracted steam by installing a steam ejector, (2) mixing a portion of flash-off water with the extracted steam to utilize the surplus heat of the extracted steam, and (3) recycling the low-temperature waste heat from the CO_2 capture process to heat the condensed water [31]. After the heat recovery, the efficiency penalty of CO_2 capture in the new integrated system decreased by 4.91 percentage points compared to the reference case [31]. The research also found that the high-stage steam substitute scheme for flue gas heat recovery saved more energy than the low-stage steam substitute scheme [32]. For the de-carbonization of natural gas combined cycle (NGCC) power plants, four measures are adopted: (1) recycling part of exhausted gas from the gas turbine to increase the CO_2 concentration in flue gas, (2) mixing a portion of condensate water from the reboiler with the extracted steam to utilize the excess heat of the extracted steam, (3) compressing the CO_2 stream at the top of stripper to recover the latent heat for sorbent regeneration, and (4) introducing a transcritical CO_2 cycle to utilize the sensible heat in flue gas to generate electricity. The techno-economic evaluation indicated that the cost of electricity and the cost of CO_2 avoided decreased by 8.66% and 27.46%, respectively [33]. Oexmann et al. (2010) integrated waste heat from the desorber overhead condenser of the CO_2 capture unit and from the CO_2 compressor into the water-steam-cycle of the power plant, offering an optimisation option [34]. Liu et al. (2012) investigated different integration cases between the power station and the capture plant according to different positions of steam extraction from the power plant [35]. They found that optimising the heat integration between the steam cycle and the capture process can significantly improve the overall energy efficiency of the power plant, with the efficiency penalty of the best integration case decreasing to 9.75% from the reference case of 12.3%. Wang et al. (2015) proposed extracting a portion of the water vapor and its latent heat from flue gases using a nanoporous ceramic membrane capillary condensation separation mechanism [36]. The waste heat from the power plant boiler system of a pulverised fuel power plant can also be recovered to provide up to 100% of the heat required for solvent regeneration, significantly reducing the efficiency penalty of CO_2 capture process [37].

Integration of renewable energy and CO_2 capture power plant can achieve lower energy penalty than other integration approaches (categories 1 and 2). In comparison to other renewables, such as wind power and photovoltaics, solar thermal with heat storage can provide steady energy under variable environmental conditions. In terms of technical feasibility, two promising options are the solar-assisted high-pressure feedwater heating and solar-assisted reboiler heating. Therefore, the integration of solar energy is chosen as a strategy to improve performance. Mokhtar et al. (2012) proposed and theoretically evaluated a system for reducing the power plant output reduction by providing part of the PCC energy input using solar-thermal energy. Fresnel concentrators were considered in the study, which showed that the output power penalty was reduced, and that the proposed technology was feasible from the perspectives of thermal efficiency and economy [38]. Zhao et al. (2012) integrated a parabolic-trough solar thermal system with an MEA-based CO_2 capture process in a 600-MW coal-fired power plant [39]. The capture subsystem was modelled and simulated in Aspen Plus software, with the hybrid system having potentially less output power penalty and lower cost. Zhai et al. (2017) proposed three different configurations for integrating a 1000 MW coal-fired power plant with solar energy system and a post-combustion CO_2 capture system [40]. The main difference between the three systems was that the solar thermal was used to replace the first extraction to heat the feed water, or to provide the MEA regeneration heat demand. The best option proved to be using solar thermal to replace the first high-pressure extraction and using part of the intermediate-pressure cylinder exhaust to provide the reboiler heat demand. Wang et al. (2017) performed a life cycle analysis of a 300 MW solar-assisted post-combustion CO_2 capture processes [41]. Three cases were analysed: base case integrated with CO_2 capture process; base case integrated with CO_2 capture and solar-assisted reboiler heating process; and base case extended to CO_2 capture and solar-assisted repowering process. This showed that the solar-assisted repowering scheme has better performance with regard to cost, with superior life cycle, greenhouse gas reduction rate, and life cycle cost of energy removed. Wang et al. (2017)

developed a pilot test system with solar-assisted post-combustion carbon capture to study the system performance [42]. Parabolic trough and linear Fresnel reflector solar thermal collector systems were tested. Results showed that solar collectors can provide the required thermal energy for the reboiler, and the integration system was demonstrated to be technically feasible.

For these three categories, integrating solar-aided CO_2 capture offers a method of providing the energy requirements of the CO_2 capture process using external and near-zero emission energy [42]. In most studies, the CO_2 capture system was researched from the perspectives of energy and efficiency performance. The CO_2 capture system was evaluated with respect to its energy aspects [43], techno-economic aspects [44–46] and environment effects aspects [47]. System integration of solar thermal and power generation with CO_2 capture is complex and worth further study, especially regarding the combination of exergy performance and economic performance, which can be used to evaluate the exergy and thermo-economic cost of each stream and identify improvement.

Thermo-economic structural theory, which is based on the second law of thermodynamics, is a powerful tool for exergy analysis, thermo-economic study and performance evaluation of an energy system [48]. The thermo-economic structural theory method has great advantages in the analysis of complex energy systems, having a broad application field, which includes system optimisation and troubleshooting, and is easy to combine with other methods. In the thermo-economic structural theory method. The thermodynamic performance and economic performance of the system are correlated in order to be studied, rather than being researched separately. Moreover, the exergy cost and thermo-economic cost of each flow can be obtained. In a previous study, we improved the analysis method for condensers to make thermo-economic analyses more comprehensive, and compared solar-aided coal-fired power plants in two modes (fuel saving and power boosting) [48]. This study proved that the improved thermo-economic analysis can be used to evaluate complex energy systems.

In the current study, we extend our previous work to investigate the integration of solar energy systems with a 1000 MW power plant and an MEA-based CO_2 capture in two configurations. The first is the integration of solar-aided coal-fired power generation with MEA-based CO_2 capture, termed SA-PG-CC. In this configuration, high-pressure extraction steam from the turbine is replaced by solar thermal to heat the feed water, while the low-pressure extraction steam is used to heat the stripper reboiler. The second configuration involves the integration of solar energy system with MEA-based CO_2 capture in coal-fired power generation (SA-CC-PG), in which solar thermal replaces the low-pressure extraction steam to heat the stripper reboiler. The two configurations are compared with the baseline coal-fired power generation with MEA-based CO_2 capture, termed PG-CC, in which the low-pressure extraction steam is used to heat the stripper reboiler without the introduction of solar thermal. To mitigate the efficiency penalty caused by carbon capture, SA-PG-CC and SA-CC-PG are two different ways of using solar thermal energy in power plants with CO_2 capture. The aim of this study is to assess the thermo-economic performance of these two configurations and to identify further system improvements from a thermo-economic point of view.

2. System Description

2.1. MEA-Based Post-Combustion CO_2 Capture Process

Figure 1 shows the MEA-based post-combustion CO_2 capture process. The flue gas discharged from the boiler is sent to the absorber bottom after pre-treatment, which includes deNO_x, electrostatic precipitation, desulfurization and direct-contact cooling. The MEA solution enters the absorber from the top and is brought into contact with the flue gas flowing from the bottom through the gas and liquid distributors and internal packing materials (either random or structured). After CO_2 capture, the flue gas is washed and removed via the chimney exhaust. The CO_2-rich solvent is pumped into the top of the stripper after exchanging heat with the CO_2-lean solvent from the stripper reboiler. The CO_2-rich solvent in the stripper is further heated in the reboiler and desorbed to release the CO_2. In this way, the MEA solution is regenerated and continues to capture CO_2 in the absorber.

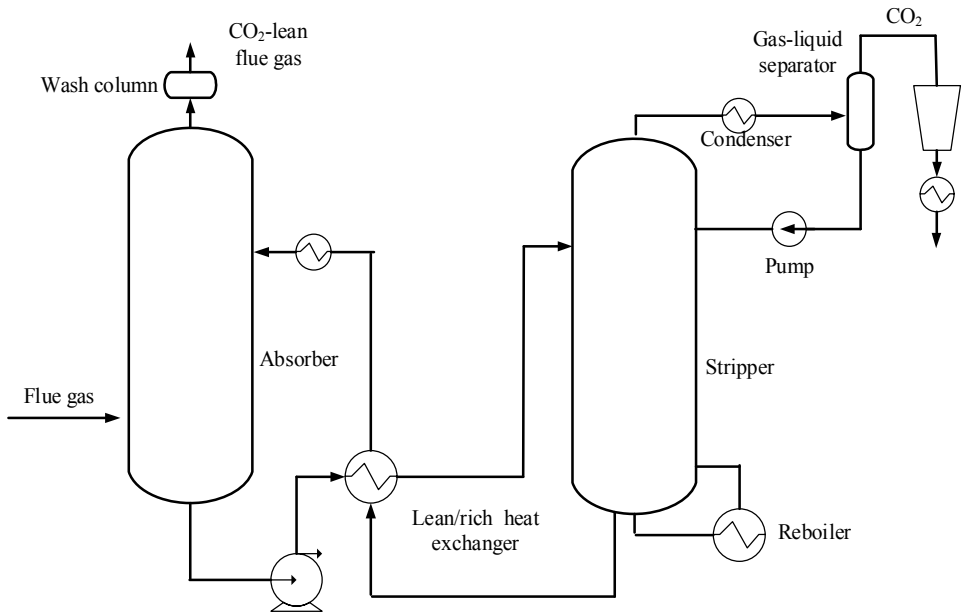

Figure 1. Monoethanolamine-based post-combustion CO_2 capture process.

2.2. Solar-Aided Coal-Fired Power Generation with CO_2 Capture

The 1000 MW SA-PG-CC system is shown in Figure 2. It consists of three subsystems: (i) a parabolic-trough solar collector, (ii) MEA-based CO_2 capture, and (iii) coal-fired power generation.

In the SA-PG-CC system, the parabolic-trough solar collector is coupled with coal-fired power generation in a similar way as the SA-PG system in [25]. The MEA-based CO_2 capture subsystem is directly integrated with the power station through the steam extraction. Sunlight is reflected into the heat absorption tube by parabolic-trough solar collectors, heating the thermal oil in the tube. In the oil–water heat exchanger (OWHE), feed water is heated by the thermal oil, rather than the first extraction steam from the high-pressure turbine. A flow of extracted steam from the low-pressure turbine is used to heat the CO_2-rich solution in the reboiler of the stripper, allowing CO_2 to be released and the MEA solution to be regenerated. After releasing heat in the reboiler, the extraction steam is sent to the condenser at the turbine exhaust, where it continues to be used in the steam cycle.

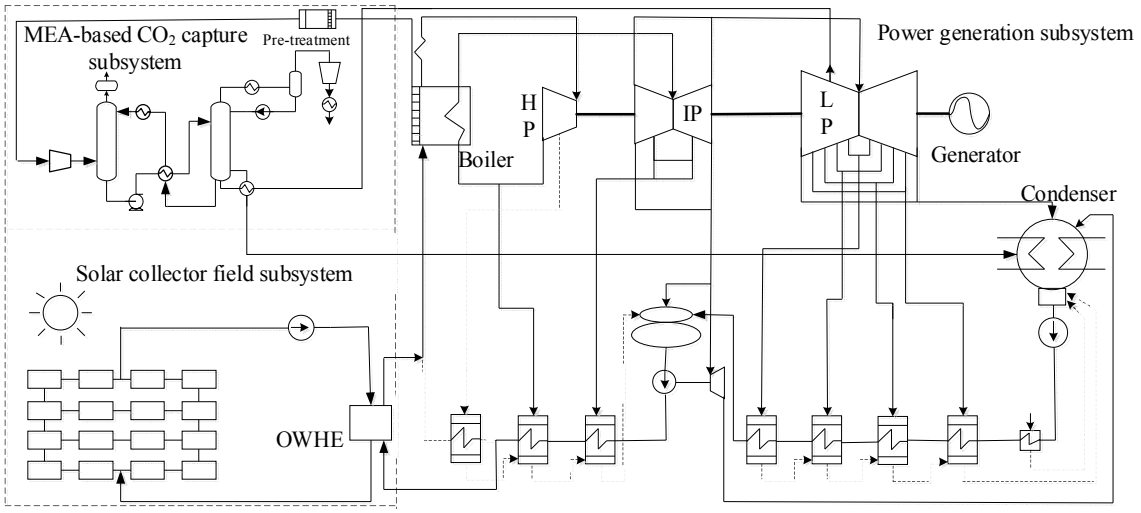

Figure 2. Solar-aided coal-fired power generation with CO_2 capture (SA-PG-CC) system.

2.3. Solar-Aided CO_2 Capture Coal-Fired Power-Generation System

Figure 3 shows the 1000 MW SA-CC-PG system, which has the same three subsystems as SA-PG-CC, but in a different configuration. The SA-CC-PG system integrates the parabolic-trough solar-collector subsystem with MEA-based CO_2 capture and uses solar thermal to supply heat to the stripper reboiler. This is achieved by circulating the thermal oil between the solar energy system and the CO_2 capture system. The thermal oil is heated in the solar energy system and then pumped through the stripper reboiler to exchange heat with the rich MEA solvent. After that, the oil returns to the solar energy system and continues the cycle.

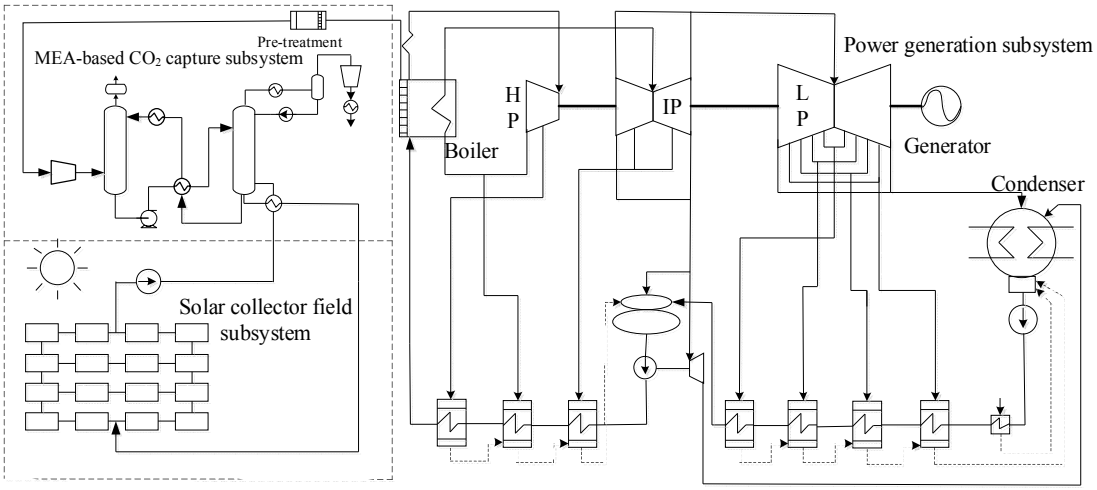

Figure 3. Solar-aided CO_2 capture coal-fired power generation (SA-CC-PG) system.

2.4. Reference System

The reference system is a 1000 MW coal-fired power-generation system with MEA-based CO_2 capture (PG-CC), as shown in Figure 2, but without the solar collector subsystem. A flow of extraction steam from the low-pressure turbine provides the heat required by the stripper boiler.

The coal-fired power-generation subsystem consists of a boiler, a turbine, a generator, a condenser, feed-water heaters and a deaerator. The boiler includes a superheater (SH) and a reheater (RH). The turbine is an N1000-25/600/600 type and consists of high-pressure cylinders (HP), intermediate-pressure cylinders (IP) and low-pressure cylinders (LP). The cylinders are divided from their extraction points to facilitate analysis. Feed-water heaters include three high-pressure reheaters (HTR1-3), four low-pressure reheaters (HTR4-7), and a deaerator (DTR).

The components' ID numbers and abbreviations are shown in Appendix A.

3. Modelling and Method

In this section, we establish the modelling of the system and introduce the method of thermo-economic structural theory.

3.1. System Modelling

The subsystems in the model are (i) a parabolic-trough solar-collector field, (ii) power generation, and (iii) MEA-based CO_2 capture. The main calculation process is briefly introduced. This study is based on a design point system. The seasonal effects and variable irradiation condition are not considered yet. One of the advantages of the solar thermal system is its stability in dealing with different irradiation conditions, particularly for a system configured with a thermal energy storage system. If there is insufficient solar energy to meet the heating requirements for the integration, the extracted steam can be used as a supplement.

3.1.1. Solar Field Subsystem

The heat input into the fluid flow is given by:

$$Q_{HTF} = m_{HTF}(h_{out} - h_{in}) \tag{1}$$

where Q_{HTF} is the heat absorbed by the heat transfer fluid, m_{HIF} is the mass flowrate of the heat transfer fluid, and h_{out} and h_{in} are the outlet and inlet enthalpy of the heat transfer fluid, respectively.

The available heat input Q_{eff} depends on the solar heat input Q_{solar}, the thermal losses of the receivers $Q_{receiver}$ and the field piping Q_{pipe}:

$$Q_{\text{eff}} = Q_{solar} - Q_{receiver} - Q_{pipe} \tag{2}$$

The solar input Q_{solar} is determined by:

$$Q_{solar} = DNI \cdot A_{net} \cdot f_{opt} \cdot k \cdot f_{shading} \cdot f_{end} \cdot f_{wind} \cdot f_{clean} \tag{3}$$

where DNI is the direct normal irradiation, A_{net} is the net aperture area, f_{opt} is the peak optical efficiency, k is the incident angle correction, $f_{shading}$ is the factor to include shading losses, f_{end} is the factor to correct end loss effects, f_{wind} is the factor to include optical losses due to wind impact, and f_{clean} is the factor to correct for actual mirror cleanliness.

3.1.2. Power-Generation Subsystem

The thermal process in the boiler is calculated as:

$$Q_b = m_b(h_{b,out} - h_{b,in})\eta_b \tag{4}$$

where Q_b is the thermal energy provided by coal fuel, m_b is the mass flowrate of feed water, $h_{b,in}$ and $h_{b,out}$ are the specific enthalpy of feed water at the boiler inlet and steam at the boiler outlet, respectively, and η_b is the thermal efficiency of the boiler.

The thermal process in the turbine is calculated by:

$$W = m_t(h_{t,in} - h_{t,out})\eta_t \tag{5}$$

where W is the work done by steam in the steam turbine, m_t is the mass flowrate of steam into the steam turbine, $h_{t,in}$ and $h_{t,out}$ are the specific enthalpy of the steam inlet and outlet of the turbine, respectively, and η_t is the relative internal efficiency of the steam turbine.

3.1.3. MEA-Based CO_2 Capture Subsystem

The chemical model used in the MEA-based CO_2 capture subsystem include the following equilibrium and kinetic reactions.

$$\text{Equilibrium: } 2H_2O \leftrightarrow H_3O^+ + OH^-$$

$$\text{Equilibrium: } CO_2 + 2H_2O \leftrightarrow H_3O^+ + HCO_3^-$$

$$\text{Equilibrium: } HCO_3^- + H_2O \leftrightarrow CO_3^{2-} + H_3O^+$$

$$\text{Equilibrium: } MEAH^+ + H_2O \leftrightarrow MEA + H_3O^+$$

$$\text{Kinetic: } CO_2 + OH^- \rightarrow HCO_3^-$$

$$\text{Kinetic: } HCO_3^- \rightarrow CO_2 + OH^-$$

$$\text{Kinetic: } MEA + CO_2 + H_2O \rightarrow MEACOO^- + H_3O^+$$

$$\text{Kinetic: } MEACOO^- + H_3O^+ \rightarrow MEA + CO_2 + H_2O$$

The detailed description of the capture system can be found in our previous publication [16].

The CO_2 removal ratio is the molar ratio of the absorbed CO_2 from the flue gas to the total CO_2 content in the flue gas:

$$\eta_{removal} = 1 - \frac{n_{co_2-cleangas}}{n_{co_2-fluegas}} \tag{6}$$

The CO_2 loading (η_{load}) is defined as the molar ratio of CO_2 to MEA in the absorbent solution:

$$\eta_{load} = \frac{n_{co_2} + n_{MEACOO^-} + n_{HCO_3^-} + n_{CO_3^{2-}}}{n_{MEA} + n_{MEA^+} + n_{MEACOO^-}} \tag{7}$$

where n is the number of moles of each component in the solution.

3.2. Thermo-Economic Structural Theory

The thermo-economic structural theory used in this paper is detailed in [28], and is only briefly described in this section.

Physical structure models are established to simulate the SA-PG-CC and SA-CC-PG systems. The physical structures are used to describe the relations of streams and components from matter and energy points of view. The productive structure is an abstract expression of the actual material flow using the concept of fuel and products to describe the productive function of components and their connections. The exergy cost of each flow is analysed according to the results of the physical model of the system. Non-energy factors, such as investment, are introduced, and the thermo-economic cost of each component is analysed according to the corresponding productive model [48–50].

3.2.1. Physical and Productive Structures

Figure 4 shows the physical structure of the 1000 MW SA-PG-CC system. The physical structure can be obtained by dividing up the system according to component function. Inflows and outflows represent substances and exergy flows. The boiler is divided into a superheater (9) and a reheater (10). The steam turbine is divided into different components (11–19). The feed-water heaters (1–8), the deaerator (5), the condenser (23) and the pumps (21, 22, 26) are not divided, because the calculation accuracy satisfies the requirements. The parabolic-trough solar-collector subsystem consists of collectors (25) and a pump (26). The MEA-based CO_2 capture subsystem is associated with the whole system via the stripper reboiler system (27).

Figure 5 shows the physical structure of the 1000 MW SA-CC-PG system. It consists of the same subsystems as SA-PG-CC, but in a different configuration.

In this thermo-economic structural theory, a component is produced according to its function. The concepts of fuel and product are used to construct the corresponding productive structure model and describe the function of each flow. The quantified representation of the production results is defined as product (P), and it can be energy or matter. The fuel (F) is the exergy consumed for the product [48–51]. The function of the condenser is to return the working fluid to the starting point of the cycle, reducing the entropy of the working fluid. Its product is negentropy (FS) [48–51], which is equal to the entropy of the working fluid reduced in the condenser, and can be calculated as:

$$FS = T_0(S_{in} - S_{out}) \tag{8}$$

where T_0 is the temperature of the environment, and S_{in}, S_{out} are the entropy of the inlet and outlet flow, respectively. Each component consumes two fuels: exergy (FB), used for production, and entropy, which is increased in this process. The productive structure diagram can express the relationship between the flows of components from the perspectives of fuel and product.

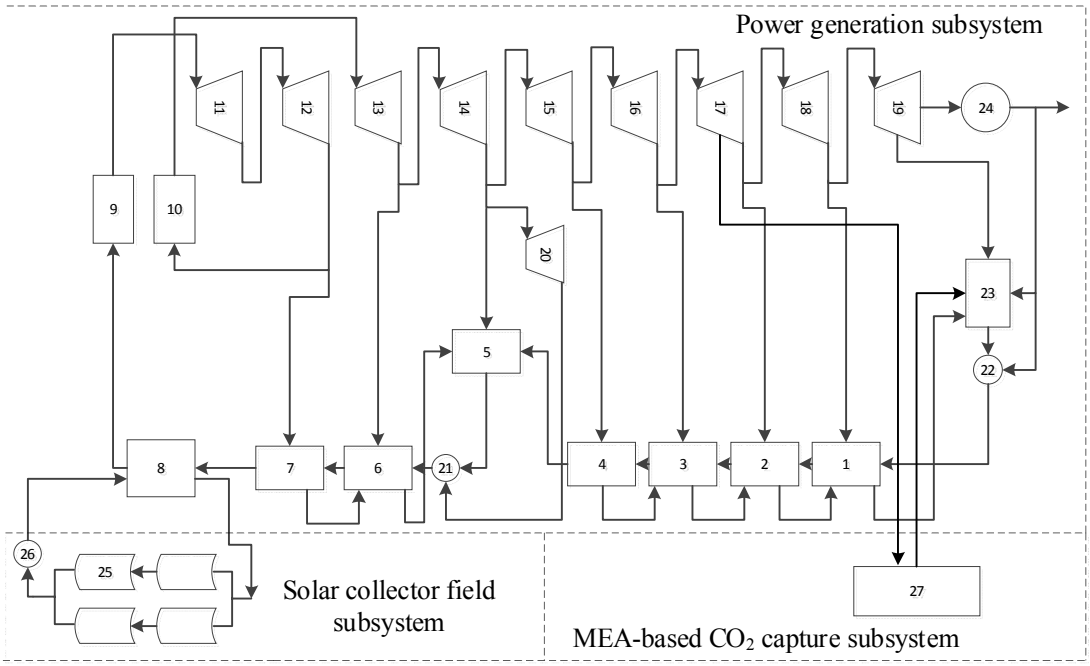

Figure 4. Physical structure of the solar-aided coal-fired power generation with CO_2 capture (SA-PG-CC) system.

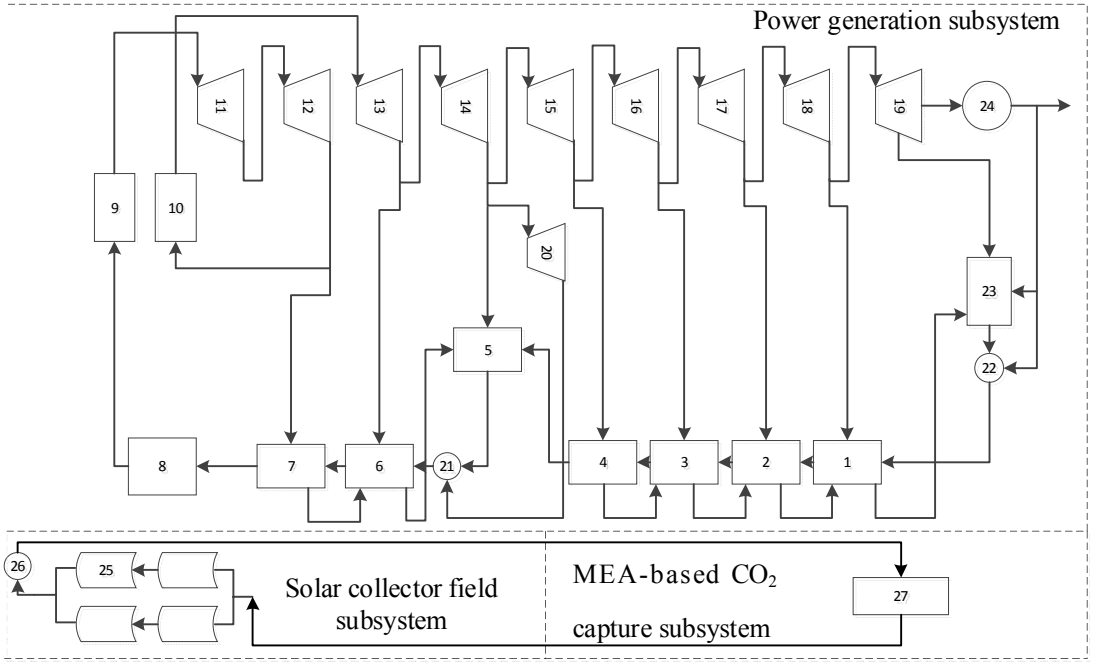

Figure 5. Physical structure of the solar-aided CO_2 capture coal-fired power generation (SA-CC-PG) system.

Figures 6 and 7 show the productive structures of the 1000 MW SA-PG-CC and 1000 MW SA-CC-PG systems, respectively. In these figures, the inlet flow of the pooled component (J) signifies the collection of products from other components. The outflow of the dispersion component (O) refers to distribution of fuels to other components.

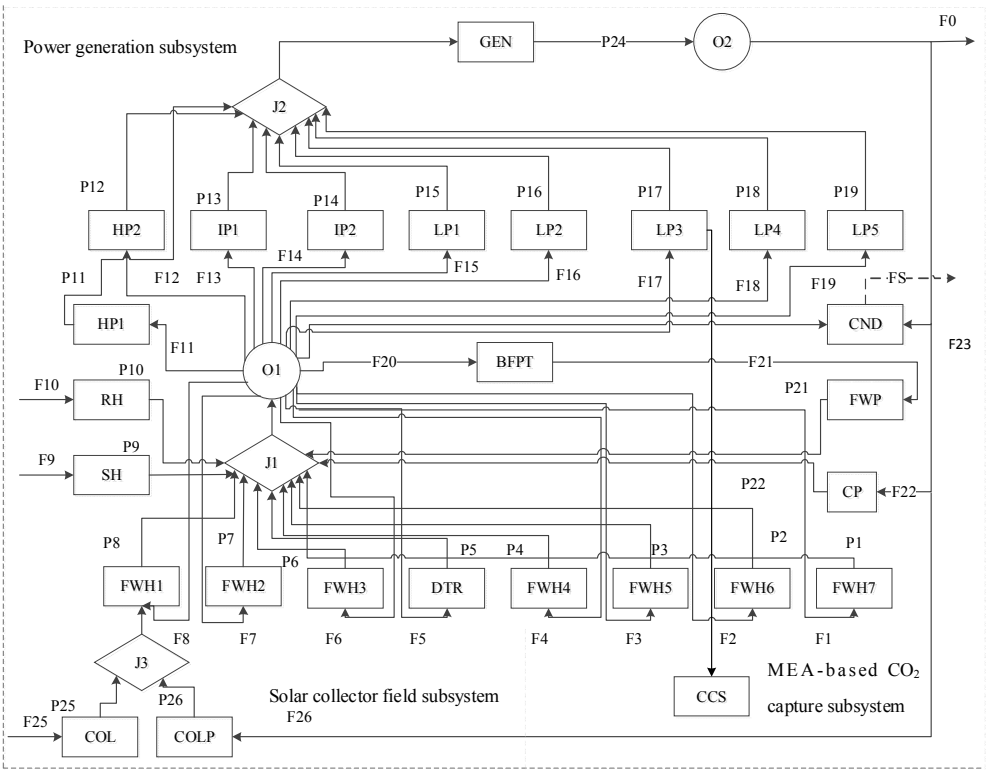

Figure 6. Productive structure of the solar-aided coal-fired power generation with CO_2 capture (SA-PG-CC) system.

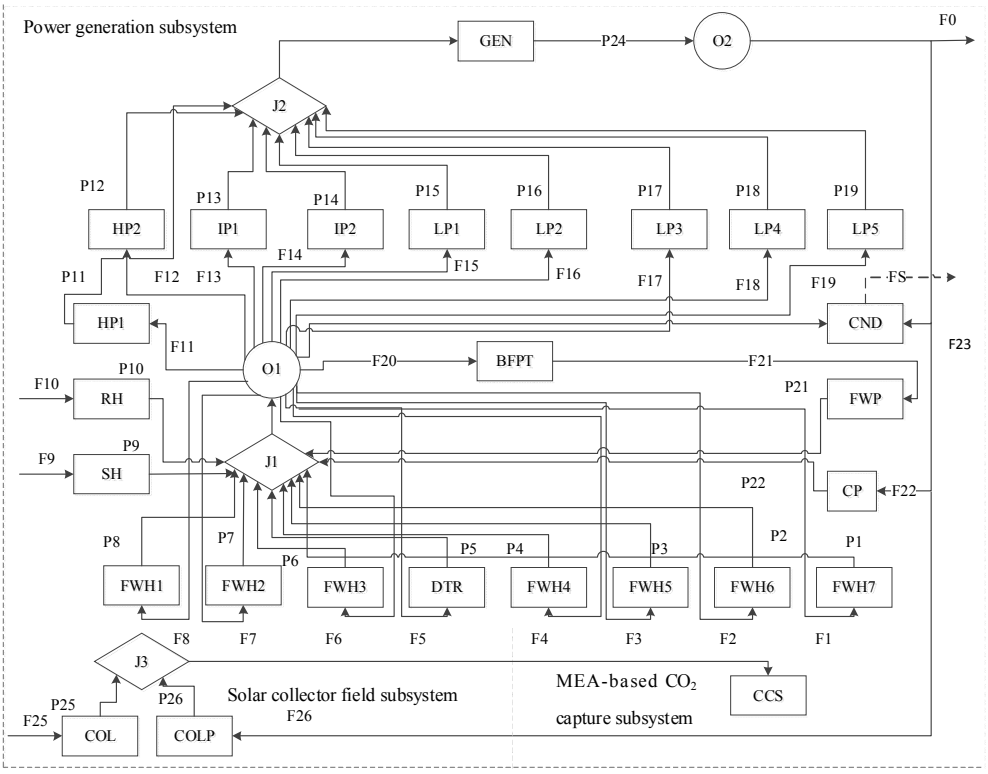

Figure 7. Productive structure of the solar-aided CO_2 capture coal-fired power generation (SA-CC-PG) system.

3.2.2. Exergy Cost Model

Exergy cost B^* of a flow refers to the external exergy of the system (coal fuel, Etc.) consumed for the product B. Unit exergy cost k^* signifies the external exergy consumed for the unit product B:

$$k^* = \frac{B^*}{B} \tag{9}$$

kB and kS signify the fuel exergy and negentropy consumed for the unit product B, respectively. The exergy cost equation can be obtained by:

$$k^*_{P,i} = kB_i k^*_{FB,i} + kS_i k^*_{FS,i} \quad i = 0, 1, n \tag{10}$$

kI represents the irreversible exergy loss in the process of producing the unit product P. There is $kB_i = 1 + kI_i$. The exergy cost equation can be expressed as exergy cost of fuel k^*_{FB}, exergy cost of irreversible $kI_i k^*_{FB,i}$ and exergy cost of negentropy $kS_i k^*_{FS,i}$, which describes the exergy cost caused by fuel, irreversible loss and negentropy:

$$k^*_{P,i} = k^*_{FB,i} + kI_i k^*_{FB,i} + kS_i k^*_{FS,i} \quad i = 0, 1, n \tag{11}$$

3.2.3. Thermo-Economic Cost Model

On the basis of the analysis of the exergy cost model, the thermo-economic cost model takes into consideration the factors of coal price, equipment investment and operation and maintenance cost. The thermo-economic cost C represents the total amount of money consumed for product P. Unit thermo-economic cost c (\$/kJ) represents the total amount of money consumed for unit product: $c = C/P$. Non-energy costs are denoted as Z, including the monetary cost of the fuel consumed, investment and operation cost of the system.

$$c_{pi} \cdot P_i = \sum_{j=1}^{n} c_{F_j} \cdot F_j + \xi \cdot Z_j \tag{12}$$

In which the ξ is the levelized factor and Z_j is investment cost of the component.

Non-energy costs are added to the exergy cost model. Unit thermo-economic cost can be expressed as the thermo-economic cost of fuel ($c_{FB,i}$), thermo-economic cost of irreversibles ($c_{I,i}$), thermo-economic cost of negentropy ($c_{N,i}$) and thermo-economic cost of investment ($c_{Z,i}$).

$$c_{P,i} = c_{FB,i} + c_{I,i} + c_{N,i} + c_{Z,i} \tag{13}$$

3.2.4. Levelized Cost of Electricity Model

Levelized cost of electricity (LCOE) is calculated as [52,53]:

$$LCOE = \frac{TCR \cdot FCF + O\&M + FC}{E_{coal} + E_{solar}} \tag{14}$$

$$FCF = \frac{r(1+r)^t}{(1+r)^t - 1} \tag{15}$$

where TCR is the total capital requirement of the power plant after integration, including the purchased equipment delivered costs, total direct costs, total indirect costs, profit, and contingency; FCF is the fixed charge factor; r is the interest rate; $O\&M$ is the annual operating and maintenance expenditure; FC is the fuel cost; t is the economic life of the plant; E_{coal} and E_{solar} are the annual electricity output from coal fuel and solar thermal, respectively.

3.2.5. Model Solution

In this paper, the models for the parabolic-trough solar subsystem and coal-fired power-generation subsystem were established in EBSILON® Professional 13.00. This software is widely applied in the calculation, design and optimisation of thermodynamic systems. On the basis of the correct formula, the mass and energy conservation of the thermodynamic process can be accurately calculated [54–56]. The simulation results have been validated and used in thermodynamic calculations, indicating that the simulation results from EBSILON® Professional are reliable [57–60]. The MEA-based CO_2 capture subsystem was modelled and simulated using Aspen Plus. This software simulates chemical processes based on mass conservation, energy conservation, chemical equilibrium and kinetics, and is widely applied in chemical process research [38,61–64]. The thermodynamic and transport properties of the MEA-based CO_2 capture process were simulated using the electrolyte-NRTL model [50]. The process in Aspen Plus is shown in Figure 8. The level of detail is the same as that shown in Figure 1. According to the simulation results, the parameters of the physical structure model and the productive structure model were obtained. The exergy cost equation and thermo-economic cost equation of each component were solved simultaneously to obtain the results of the thermal-economic analysis.

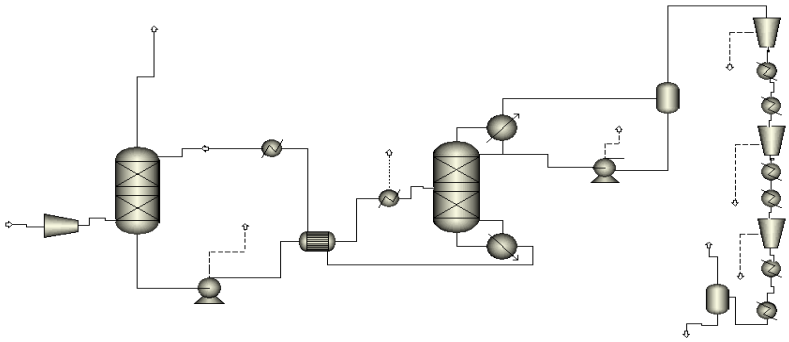

Figure 8. The model flowsheet in Aspen Plus.

The exergy cost equation and thermo-economic cost equation of each component are shown in Table 1 [48,50], and the model procedure for the analysis is shown in the Figure 9. The baseline coal-fired power plant model before extraction for the CO_2 capture process is established first. Then the corresponding MEA-based post-combustion CO_2 capture process model can be determined. With the baseline coal-fired power plant model and the CO_2 capture process model, the coal-fired power plant model after extraction for the CO_2 capture process can be obtained. Then the baseline PG-CC system can be configured, and the solar collector field models for SA-PG-CC and SA-CC-PG can be calculated. The SA-PG-CC system can be solved with the PG-CC system and the solar collector field model. The SA-CC-PG system can be solved with the baseline coal-fired power plant model before extraction for the CO_2 capture process, the CO_2 capture process model and the solar collector field model. Therefore, the exergy cost analysis and thermo-economic cost analysis can be carried out.

Table 1. Exergy cost equation and thermo-economic cost equation.

Component	Number	Exergy Cost Equation	Thermo-Economic Cost Equation
FWH, OWHE, DTR	1–8	$k^*_{P,i} = kB_i k^*_{FB,i} + kS_i k^*_{FS,I}$	$c_{P,i} = kB_i c_{FB,i} + kS_i c_{FS,i} + kZ_i$
SH, RH	9,10	$k^*_{P,i} = kB_i k^*_{Fuel} + kS_i k^*_{FS,I}$	$c_{P,i} = kB_i c_{Fuel} + kS_i c_{FS,i} + kZ_i$
HP, IP, LP, BFPT	11–20	$k^*_{P,i} = kB_i k^*_{FB,i} + kS_i k^*_{FS,I}$	$c_{P,i} = kB_i c_{FB,i} + kS_i c_{FS,i} + kZ_i$
FWP, CP	21,22	$k^*_{P,i} = kB_i k^*_{P,24} + kS_i k^*_{FS,i}$	$c_{P,i} = kB_i c_{P,24} + kS_i c_{FS,i} + kZ_i$
CND	23	$k^*_{P,23} = kB_{23} k^*_{FB,23} + kW_{kW,23} k^*_{FW,23}$	$c_{P,23} = kB_{23} c_{FB,23} + kW_{23} c_{FW,23} + kZ_{23}$
GEN	24	$k^*_{P,24} = kB_{24} k^*_{P,27}$	$c_{P,24} = kB_{24} c_{P,27} + kZ_{24}$
COL	25	$k^*_{P,25} = kB_{25} k^*_{FB,25}$	$c_{P,25} = kZ_{25}$
COLP	26	$k^*_{P,26} = kB_{26} k^*_{P,24}$	$c_{P,26} = kB_{26} c_{P,24} + kZ_{26}$
J1	27	$k^*_{P,27} = \sum r_i k^*_{P,i}$	$c_{P,27} = \sum r_i c_{P,i}$
J2	28	$k^*_{P,28} = \sum r_i k^*_{P,i}$	$c_{P,28} = \sum r_i c_{P,i}$
J3	29	$k^*_{P,29} = \sum r_i k^*_{P,i}$	$c_{P,29} = \sum r_i c_{P,i}$
O1	30	$k^*_{FB,j} = k^*_{P,27}$	$c_{FB,j} = c_{P,27}$
O2	31	$k^*_{FB,0} = k^*_{FW,23} = k^*_{FB,21,22} = k^*_{P,24}$	$c_{FB,0} = c_{FW,23} = c_{FB,21.22} = c_{P,24}$

Note: BFPT = feed-water pump turbine; SH = boiler superheater; CND = condenser; COL = collector; COLP = collector oil-pump; CP = condenser water pump; DTR = deaerator; FWH = feed-water heater; FWP = feed-water pump; GEN = generator; HP = high-pressure turbine; IP = intermediate-pressure turbine; J = pooled component; O = dispersion component; LP = low-pressure turbine; OWHE = oil–water heat exchanger; RH = reheater.

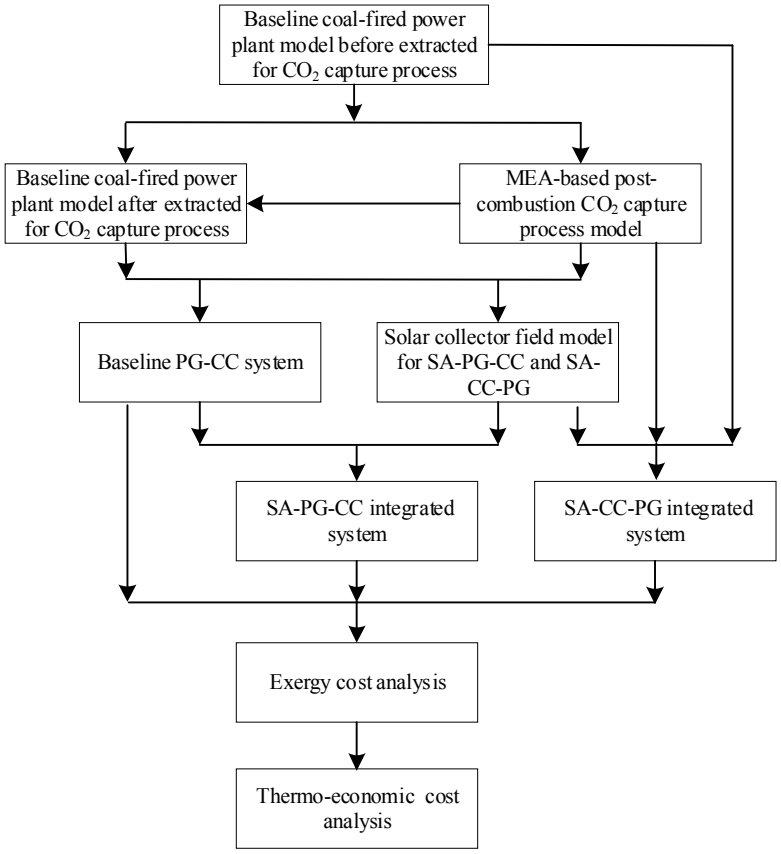

Figure 9. The model procedure for the analysis.

4. Case Study

4.1. Basic Data

4.1.1. Technical Parameters

The coal-fired power-generation subsystem is a 1000 MW coal-fired power plant with main parameters as listed in Table 2. We have assumed that the three systems (SA-PG-CC, SA-CC-PG and

PG-CC) consume the same amount of coal per hour, and therefore produce the same amount flue gas and use the same CO_2 capture process. Table 3 shows the main parameters of the parabolic-trough solar-thermal subsystem; the data is the design data of the solar collector field of the solar-aided coal-fired demonstration plant in Gansu Province, China [65]. Table 4 shows the flue gas, absorber and stripper parameters. The inlet and outlet temperature of the solar collector field is the temperature of the thermal oil that is used to heat the feedwater and reboiler in the SA-PG-CC and SA-CC-PG, respectively. In the SA-CC-PG, the thermal oil is heated in the solar energy system and then enters the stripper reboiler to exchange heat with the rich MEA solvent. The hot thermal oil temperature is 217 °C. It should be pointed out that this is the temperature of the heat source, not the solvent in the stripper. Additionally, the solvent temperature is controlled to not exceed 125 °C by design of the reboiler.

Table 2. Main design parameters of the coal-fired power plant subsystem.

Parameter	Value	Unit
Capacity	1000	MW
Parameters of main steam	25/600/600	MPa/°C/°C
Feed-water mass flow rate	2733.43	t/h
Condenser pressure	5	kPa
Feed-water temperature	294.75	°C
Designed coal consumption rate	268	g/kWh

Table 3. Main parameters of the trough solar-collector subsystem.

Parameter	Values	Unit
Direct normal irradiation (DNI)	805	W/m^2
Inlet temperature of the solar collector field	280/123	°C
Outlet temperature of the solar collector field	387/217	°C
Peak optical efficiency of collector	0.73	–
Endloss factor	0.97	–
Shading factor	1	–
Wind factor	0.98	–
Focal length	1.71	m

Table 4. Flue gas, absorber and stripper parameters.

Flue Gas Composition	Mole per Cent	Unit	Flue Gas Composition	Mole per Cent	Unit
H_2O	10	%	O_2	3.6	%
CO_2	14	%	Temperature	40	°C
N_2	72.4	%	Pressure	0.12	Mpa
Absorber	**Value**	**Unit**	**Stripper**	**Value**	**Unit**
Number of stages	8	–	Number of stages	8	–
Top pressure	101	kPa	Reboiler pressure	220	kPa
Bottom pressure	111	kPa	Condenser pressure	210	kPa
Inlet flue gas temperature	40	°C	Reboiler heat duty	637,647.92	kW
Inlet lean solvent temperature	40	°C	Rich solvent loading	0.42	–
Liquid-to-gas ratio	2.8	kg/kg	Inlet temperature *	140/217	°C
Lean solvent loading	0.29	–	Outlet temperature *	120/123	°C

* 140 °C is the inlet temperature of steam to the reboiler in SA-PG-CC. 217 °C is the inlet temperature of hot oil to the reboiler in SA-CC-PG. 120 °C is the outlet temperature of steam (water) from the reboiler in SA-PG-CC. 123 °C is the outlet temperature of thermal from the reboiler in SA-CC-PG.

4.1.2. Economic Parameters

The coal fuel price in this system is assumed to be US\$$2 \times 10^{-6}$/kJ. The relevant economic parameters of the system are shown in Table 5. The price of each component is shown in Appendix B [48,66,67].

The relevant economic parameters of the parabolic-trough solar-thermal subsystem are shown in Table 6 [68].

Table 5. Economic parameters of the coal-fired power plant subsystem.

Parameter	Value	Unit
System maintenance factor	1.06	–
Annual operating hours	8000	Hour
Amortise factor	1	–
Amortise cycle	5	Year
Annual inflation rate	0.05	–
Construction time	3	Year
Lifetime	30	Year
Interest rate	0.08	–

Table 6. Economic parameters of solar fields for solar-aided coal-fired power generation with CO_2 capture (SA-PG-CC) and solar-aided CO_2 capture coal-fired power generation (SA-CC-PG).

Parameter	SA-PG-CC	SA-CC-PG	Unit
Collector field area	558,351	2,518,165	m^2
Floor area	1,500,000	6,000,000	m^2
Cost of unit collector field area	308	308	$\$/m^2$
Cost of unit floor area	19.3	19.3	$\$/m^2$

In this paper, the investment cost of each component in the MEA-based CO_2 capture subsystem was obtained from calculations. The investment cost of components of the same type with different power output was calculated using Equation (15) [66,67]. The investment cost of a 1000 MW CO_2 capture unit was calculated based on a 500 MW CO_2 capture unit [66–69], shown in Appendix C.

$$\frac{C_i}{C_{i,ref}} = \left(\frac{W_i}{W_{i,ref}}\right)^{0.6} \tag{16}$$

4.2. Results and Discussion

4.2.1. Exergy Cost

Table 7 shows the main exergy cost model analysis results of PG-CC, SA-PG-CC and SA-CC-PG systems, with detailed results listed in Appendix D.

Table 7. Primary results of exergy analysis for coal-fired power-generation system with MEA-based CO_2 capture (PG-CC), solar-aided coal-fired power generation with CO_2 capture (SA-PG-CC) and solar-aided CO_2 capture coal-fired power generation (SA-CC-PG).

Component	PG-CC	SA-PG-CC	SA-CC-PG	Unit
Power output	838.7	895.9	1000.7	MW
Solar exergy	0	72.9	327.9	MW
Share of solar exergy	0	3.45	13.83	%
Coal exergy	2042.6	2042.6	2042.6	MW
Share of coal exergy	100	96.55	86.17	%
Coal consumption rate	319.15	303.84	267.74	g/kWh
Efficiency of the system	41.06	42.35	42.21	%
Equivalent power output of solar	–	57.2	162	MW
Equivalent solar-power generation efficiency	–	78.5	49.4	%
Share of solar-energy power output	–	6.38	16.19	%
Unit exergy cost of electricity	2.43	2.75	2.08	kW/kW
Unit exergy cost of FWH1	2.02	–	2.05	kW/kW
Unit exergy cost of OWHE	–	6.67	–	kW/kW
Efficiency of solar-collector field	–	31	31	%

In SA-PG-CC, solar thermal was used to heat the feed water, rather than the first-stage high-pressure extraction steam at a higher temperature. A flow of low-pressure extraction steam at low temperature was used to provide the heat required in the stripper reboiler. In comparison, solar thermal in SA-CC-PG provided the heat required in the stripper reboiler directly, and the low-pressure steam was not extracted.

Compared with the PG-CC system, the coal consumption rate of the SA-PG-CC and SA-CC-PG configurations decreased by 15.31 and 51.41 g/kWh, respectively. The solar thermal required in SA-CC-PG was far more than that in SA-PG-CC, which accounts for a larger share in the total input exergy of system. The exergy absorbed by the thermal oil in SA-PG-CC and SA-CC-PG was 72.9 and 327.9 MW, respectively, resulting in a system power increase of 57.2 and 162 MW, respectively. The efficiency of the system is the efficiency of the input exergy of the system (solar exergy and coal exergy) to the system power output. Both the SA-PG-CC and SA-CC-PG systems had greater power output and system efficiency than the PG-CC system, indicating that the input of solar thermal energy improved the thermal performance of system. The efficiency of the system in SA-PG-CC is 42.35%, and in SA-CC-PG it is 42.21%. The equivalent solar-power generation efficiency is the ratio of increased power output to the input solar exergy, which is 78.5% for SA-PG-CC and 49.4% for SA-CC-PG. In the SA-PG-CC system, solar sunlight is converted to a higher-temperature thermal energy, with higher exergy efficiency compared with the SA-CC-PG system. The solar thermal energy is utilized at the high-pressure extraction energy level instead of the low-pressure steam energy level, causing the differences in system efficiency and equivalent solar-power generation efficiency. This result indicates that the solar thermal energy is more fully used in the SA-PG-CC system with the same coal consumption and CO_2 capture subsystem.

The exergy efficiency of each component in the PG-CC, SA-PG-CC and SA-CC-PG systems is shown in Figure 10 In both SA-PG-CC and SA-CC-PG, the exergy efficiency of the solar collector field was very low, at 0.17 and 0.14, respectively. This was mainly due to the high optical loss of the parabolic-trough solar subsystem, resulting in low optical efficiency. In addition, some energy was dissipated as heat loss. In SA-PG-CC, the working fluid was heated to a higher temperature than in SA-CC-PG by solar thermal, the exergy efficiency of the solar subsystem was also higher.

The exergy cost composition of each component in the PG-CC, SA-PG-CC and SA-CC-PG systems is shown in Figure 11. The exergy cost is divided into three parts: (i) fuel, which represents the minimum external exergy required to obtain the unit product; (ii) irreversible, which reflects the external exergy caused by irreversibility of the process on components; and (iii) negentropy, which indicates the consumption of external resources due to negentropy consumption.

Compared with the PG-CC system, the exergy cost of each component was slightly increased in SA-PG-CC; the exergy cost of the solar-thermal subsystem was significantly higher than other components, and the unit exergy cost of the electricity increased by 13.2%. For the same component, the exergy cost of the OWHE increased significantly, from 2.02 to 6.67, compared with the HP heater FWH1. This was due to the introduction of the solar energy system in SA-PG-CC. Due to the limitation of optical efficiency and thermal efficiency of the solar-collector subsystem, the exergy cost of solar thermal was higher than coal, which was mainly caused by irreversibility. In SA-PG-CC, the solar-collector subsystem was coupled with the power-generation subsystem; the sunlight was converted into thermal energy in the system and flowed through the system. With the flow of solar thermal energy, this part of the exergy cost was distributed to other components in the power-generation process. Therefore, the unit exergy costs of electricity in SA-PG-CC were higher than in PG-CC; nevertheless, the cost from coal combustion was greatly reduced, as a result of the coal consumption rate.

Compared with PG-CC, the exergy cost of each component in SA-CC-PG did not change significantly. In SA-CC-PG, solar thermal was used to heat the stripper reboiler, and there was a small impact on the coal-fired power-generation subsystem. The inefficiency of low-pressure steam from the last stage of the steam turbine caused a slighter higher exergy cost for components in

SA-CC-PG than in PG-CC. The system's power generation was increased, so that unit exergy costs of electricity and coal combustion rate slightly decreased.

Compared with SA-CC-PG, SA-PG-CC had a higher unit exergy cost for components in the power-generation subsystem, and a lower unit exergy cost for the solar-collector subsystem. In SA-PG-CC, the solar-collector subsystem was coupled with the power-generation subsystem, so that the additional solar exergy cost was shared by the power-generation subsystem components. In SA-CC-PG, the solar-collector subsystem was coupled with the MEA-based CO_2 capture subsystem, and the additional solar exergy cost was shared by the MEA-based CO_2 capture subsystem instead of the power-generation subsystem components. For the solar-collector subsystem, solar thermal was used at a lower temperature in SA-CC-PG (120 °C–140 °C), accompanied by a higher irreversible loss. Therefore, the solar-collector subsystem had a higher unit exergy cost in SA-CC-PG than in SA-PG-CC.

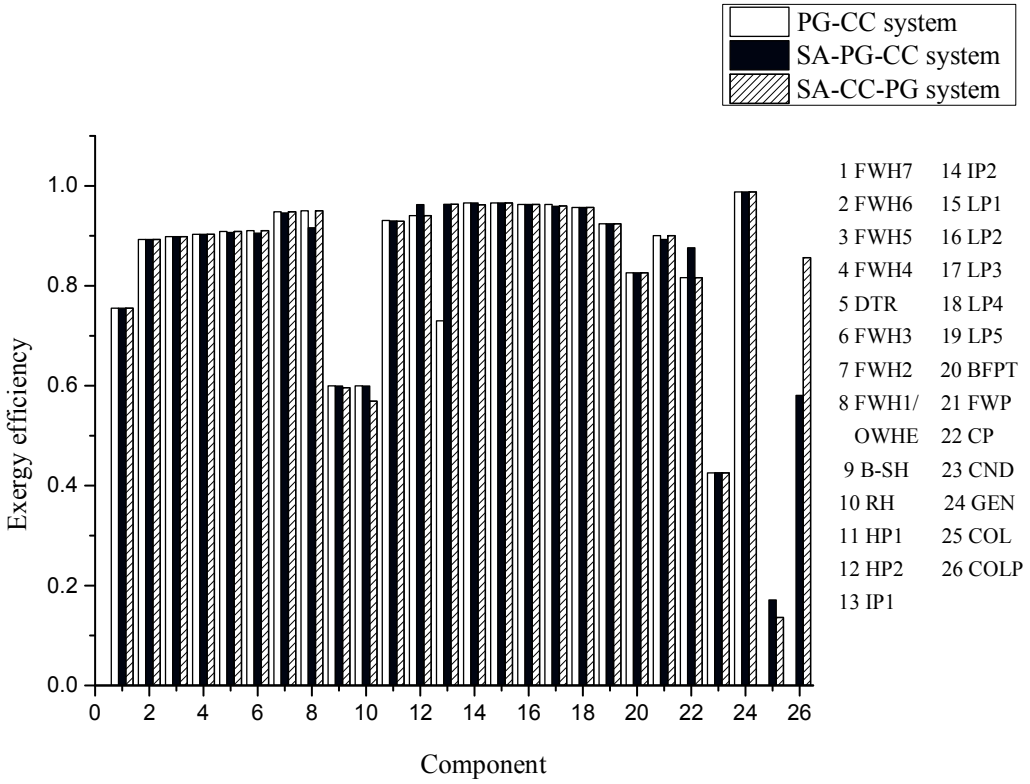

Figure 10. Exergy efficiency of each component in all three systems: coal-fired power-generation system with MEA-based CO_2 capture (PG-CC), solar-aided coal-fired power generation with CO_2 capture (SA-PG-CC) and solar-aided CO_2 capture coal-fired power generation (SA-CC-PG). Note: BFPT = feed-water pump turbine; SH = boiler superheater; CND = condenser; COL = collector; COLP = collector oil-pump; CP = condenser water pump; DTR = deaerator; FWH = feed-water heater; FWP = feed-water pump; GEN = generator; HP = high-pressure turbine; IP = intermediate-pressure turbine; LP = low-pressure turbine; OWHE = oil–water heat exchanger; RH = reheater.

Table 8 shows the main results of the MEA-based CO_2 capture subsystem's thermal performance. The three systems have the same MEA-based CO_2 capture system, with the same CO_2 removal rate and reboiler heat load. The heat required for the stripper reboiler in PG-CC and SA-PG-CC was provided by the turbine low-pressure extraction steam, with a lower exergy cost. In SA-CC-PG, the heat required for the stripper reboiler was provided by the solar thermal with a higher exergy cost. Therefore, the unit exergy cost of CO_2 in SA-CC-PG was significantly greater than in PG-CC and SA-PG-CC.

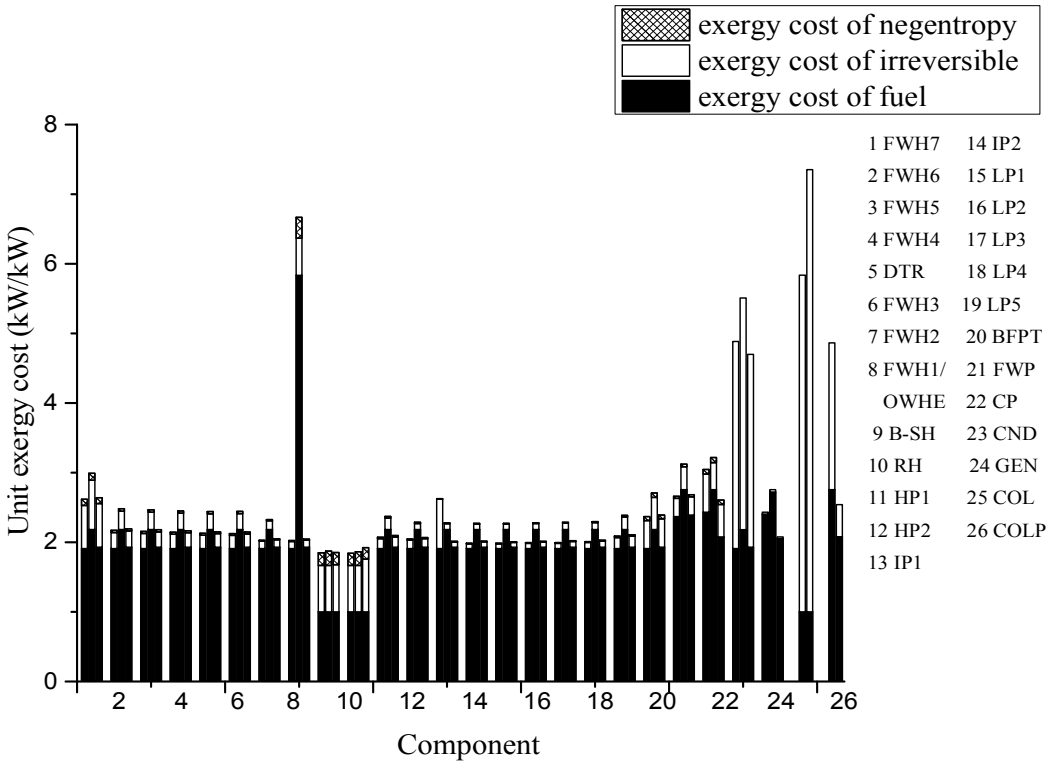

Figure 11. Exergy costs of all components in (left to right for each component): coal-fired power-generation system with MEA-based CO_2 capture, solar-aided coal-fired power generation with CO_2 capture, and solar-aided CO_2 capture coal-fired power generation. Note: BFPT = feed-water pump turbine; SH = boiler superheater; CND = condenser; COL = collector; COLP = collector oil-pump; CP = condenser water pump; DTR = deaerator; FWH = feed-water heater; FWP = feed-water pump; GEN = generator; HP = high-pressure turbine; IP = intermediate-pressure turbine; LP = low-pressure turbine; OWHE = oil–water heat exchanger; RH = reheater.

Table 8. Primary results of the MEA-based CO_2 capture subsystem for coal-fired power generation system with MEA-based CO_2 capture (PG-CC), solar-aided coal-fired power generation with CO_2 capture (SA-PG-CC) and solar-aided CO_2 capture coal-fired power generation (SA-CC-PG).

Component	PG-CC	SA-PG-CC	SA-CC-PG	Unit
Output power penalty	161.92	161.97	-	MW
Removal CO_2	199.67	199.67	199.67	kg/s
CO_2 removal rate	80.72	80.72	80.72	%
Unit CO_2 thermal consumption	3193.51	3193.51	3193.51	kJ/kg
Unit CO_2 exergy consumption	1119.75	1119.75	1303.40	kJ/kg
Unit exergy cost of heat source	1.99	2.29	5.84	kW/kW
Unit exergy cost of CO_2	2228.30	2564.23	7609.52	kJ/kg

4.2.2. Thermo-Economic Cost

The investment percentage of the solar-collector subsystem, MEA-based CO_2 capture subsystem and coal-fired power-generation subsystem in PG-CC, SA-PG-CC and SA-CC-PG is shown in Figure 12. Compared with PG-CC, the investment in the solar-collector subsystem in SA-PG-CC and SA-CC-PG increased. For SA-PG-CC, investment in the solar-collector subsystem accounts for 23%, while for SA-CC-PG it was 58% due to the larger size of the collector field.

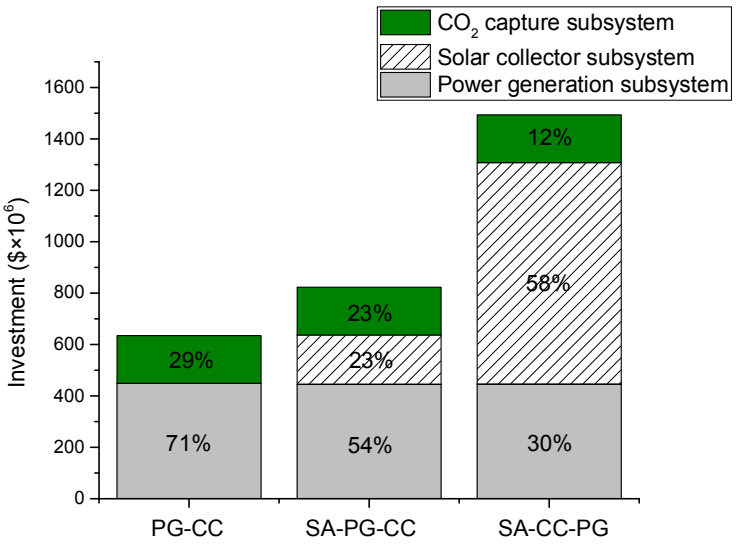

Figure 12. Investment in coal-fired power-generation system with MEA-based CO_2 capture (PG-CC), solar-aided coal-fired power generation with CO_2 capture (SA-PG-CC) and solar-aided CO_2 capture coal-fired power generation (SA-CC-PG).

Table 9 shows the main results of the thermo-economic cost model analysis for the PG-CC, SA-PG-CC and SA-CC-PG systems. Detailed results are given in Appendix E. Compared withPG-CC, the unit thermo-economic cost of electricity in SA-PG-CC was slightly increased, while the unit thermo-economic cost of CO_2 remained constant. For SA-CC-PG, the unit thermo-economic cost of electricity was slightly decreased, but the unit thermo-economic cost of CO_2 increased significantly.

In SA-PG-CC, both the power and efficiency of the system increased, but the system investment also increased, especially for the solar-collector field. Therefore, the unit thermo-economic cost of electricity slightly increased in SA-PG-CC.

In SA-CC-PG, the heat required by the stripper reboiler was provided by solar thermal. To meet the reboiler heat load, a significant increase in the solar-collector field area was required. This led to a large increase in the unit thermo-economic cost of CO_2, of which 82.25% comprised solar-collector subsystem investment. In this system, more steam can be used for power generation, thus increasing power output. As a result, the unit thermo-economic cost of electricity slightly decreased.

Table 9. Main results of the thermo-economic analysis for coal-fired power-generation system with MEA-based CO_2 capture (PG-CC), solar-aided coal-fired power generation with CO_2 capture (SA-PG-CC) and solar-aided CO_2 capture coal-fired power generation (SA-CC-PG).

Component	PG-CC	SA-PG-CC	SA-CC-PG	Unit
Total system investment	674.83	822.86	1493.92	M$
Investment of coal-fired side	448.80	445.22	445.64	M$
Share of investment of coal-fired subsystem	70.70	54.11	29.83	%
Investment of solar side	–	191.61	862.25	M$
Share of investment of solar subsystem	–	23.29	57.72	%
Investment of CO_2 capture system	186.03	186.03	186.03	M$
Share of investment of CO_2 capture system	29.30	22.61	12.45	%
Unit thermo-economic cost of feed-water heater 1 (FHW1)	8.79	–	8.38	$10^{-6}$$/kJ
Unit thermo-economic cost of oil–water heat exchanger (OWHE)	–	36.83	–	$10^{-6}$$/kJ
Unit thermo-economic cost of electricity	10.54	11.88	9.51	$10^{-6}$$/kJ
Unit thermo-economic cost of CO_2	11.16	11.16	62.64	$/t

The thermo-economic cost composition of each component in the PG-CC, SA-PG-CC and SA-CC-PG systems is shown in Figure 13, and is divided into four parts: fuel, irreversibility, negentropy and non-energy cost. The thermo-economic costs of components were mainly composed of fuel costs, in addition to the boiler, condenser and solar-collector field. For the boiler, the thermo-economic costs of negentropy and investment were also large, due to the entropy increase caused by combustion and heat transfer and equipment investment. For the condenser, the working fluid was returned to the initial state of the thermal cycle and the remaining exergy carried by the working fluid was discharged, resulting in a large number of irreversible losses. Therefore, the thermo-economic costs of the condenser mainly consisted of irreversibility. For the solar-collector field, solar thermal is considered to be free, so the very large thermo-economic cost is due to the enormous investment.

In comparison with the PG-CC system, the thermo-economic cost of components in the power-generation subsystem increased in SA-PG-CC because of the large thermo-economic cost of solar energy system. The thermo-economic cost of electricity in SA-PG-CC increased by 12.71%.

Compared with PG-CC, the system power output increased with the same power-generation subsystem in SA-CC-PG, so that each component of thermo-economic cost in the power-generation subsystem decreased. The thermo-economic cost of electricity in SA-CC-PG decreased by 9.77%.

Equation (12) was used to calculate the unit thermo-economic cost of CO_2, considering the energy-cost and the non-energy cost in the CO_2 capture process and reflecting the thermodynamic performance and economic performance. The high proportion represented by the solar-collector subsystem investment causes the great increase in the unit thermo-economic cost of CO_2 in SA-CC-PG compared with the other systems.

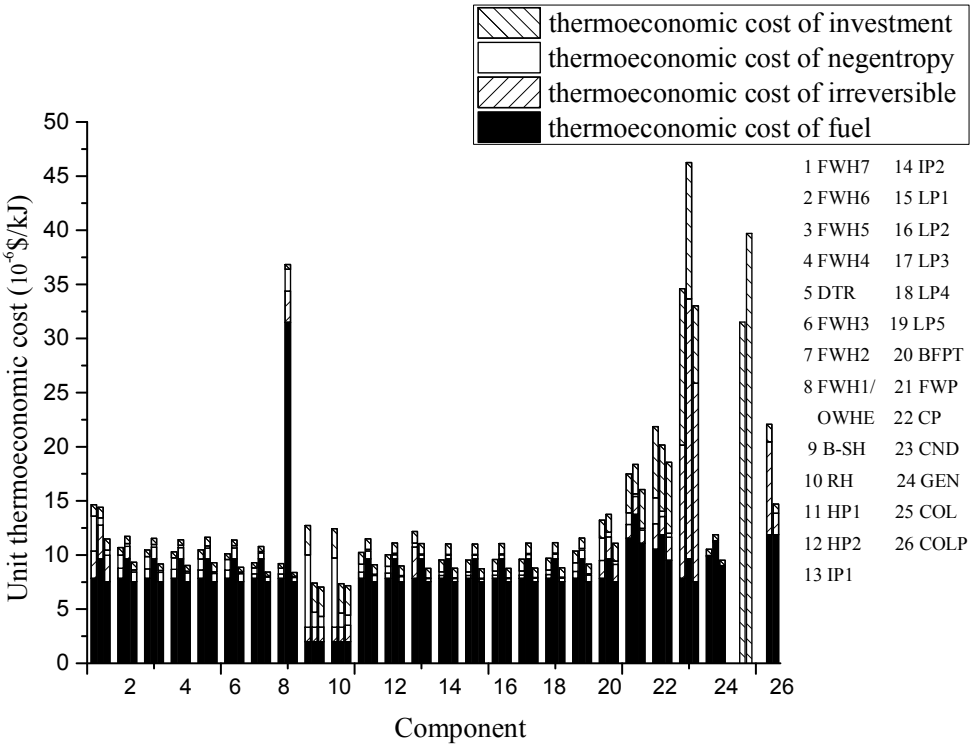

Figure 13. Composition structure of thermo-economic cost in (left to right for each component): coal-fired power-generation system with MEA-based CO_2 capture, solar-aided coal-fired power generation with CO_2 capture, and solar-aided CO_2 capture coal-fired power generation. Note: BFPT = feed-water pump turbine; SH = boiler superheater; CND = condenser; COL = collector; COLP = collector oil-pump; CP = condenser water pump; DTR = deaerator; FWH = feed-water heater; FWP = feed-water pump; GEN = generator; HP = high-pressure turbine; IP = intermediate-pressure turbine; LP = low-pressure turbine; OWHE = oil–water heat exchanger; RH = reheater.

4.2.3. Levelized Cost of Electricity

The levelized cost of electricity of three configuration systems are shown in Table 10. The LCOE of PG-CC, SA-PG-CC and SA-CC-PG are 83.32 $/MWh, 98.23 $/MWh and 165.82 $/MWh, respectively. In the thermo-economic analysis, the thermo-economic cost of electricity and CO_2 are calculated separately. The investments of solar energy subsystem are distributed into electricity or CO_2 according to the utilization of solar thermal. In the LCOE analysis, the total system costs appear in the LCOE. Although there is not much difference in the efficiency of the systems (42.35% in SA-PG-CC and 42.21% in SA-CC-PG), the required solar thermal energy is higher in SA-CC-PG. The share of solar exergy is 13.83% in SA-CC-PG, which is 3.45% in SA-PG-CC, and the equivalent solar-power generation efficiency is 49.4% in SA-CC-PG and 78.5% in SA-PG-CC. Therefore, the high-cost solar-collector field area is significantly increased in SA-CC-PG, causing a higher total capital requirement for SA-CC-PG (3235.9 M$ for SA-PG-CC and 5874.84 M$ for SA-CC-PG). There is less difference in the power output of the system, which is 895.9 MW for SA-PG-CC and 1000.7 MW for SA-CC-PG. Thus, there is a much higher LCOE for the SA-CC-PG system than for the SA-PG-CC system. This result also indicates the necessity of reducing the solar collector field cost for the large-scale use of solar thermal energy. In the PG-CC, the static capital payback period is 16 years if the electricity price is 14 cents, and 11 years if the electricity price is 16 cents. In the SA-PG-CC, the LCOE increased slightly after the introduction of solar thermal energy. The static capital payback period is 29 years if the electricity price is 14 cents and 16 years if the electricity price is 16 cents. In the SA-CC-PG, the LCOE is greatly increased and is not profitable until the electricity price reaches 16.6 cents.

Table 10. Levelized cost of electricity analysis for coal-fired power-generation system with MEA-based CO_2 capture (PG-CC), solar-aided coal-fired power generation with CO_2 capture (SA-PG-CC) and solar-aided CO_2 capture coal-fired power generation (SA-CC-PG) [53].

	Base	Factor	PG-CC	SA-PG-CC	SA-CC-PG
Purchased equipment delivered costs (PEDC/M$)			674.83	822.86	1493.92
Installation	PEDC	0.40	269.93	329.14	597.57
Piping	PEDC	0.68	458.89	559.54	1015.87
Service facilities	PEDC	0.30	202.45	246.86	448.18
Instrumentation and controls	PEDC	0.43	290.18	353.83	642.39
Total direct costs (TDC/M$)			1221.44	1489.38	2703.99
Engineering and supervision	PEDC	0.33	222.69	271.54	492.99
Construction expenses	PEDC	0.41	276.68	337.37	612.51
Total indirect costs (TIC/M$)			499.37	608.92	1105.5
Profit/M$	TDC + TIC	0.05	86.04	104.91	190.47
Contingency/M$	TDC + TIC	0.10	172.08	209.83	380.95
Total capital requirement (TCR/M$)			2653.76	3235.9	5874.84
Levelized cost of electricity ($/MWh)			83.32	98.23	165.82

4.2.4. Sensitivity Analysis

The unit thermo-economic cost of electricity and CO_2 are greatly influenced by solar-collector field investment. In this section, we discuss the influence of solar-collector field investment, and the results are shown in Figures 14 and 15. Unit solar-collector field investment is taken as $\$308/m^2$ in this study, and varies within a range of plus and minus $\$300/m^2$.

The unit thermo-economic cost of electricity in SA-PG-CC is equal to that in PG-CC when the unit solar-collector field investment is reduced by $\$179.4/m^2$ to $\$128.6/m^2$ (Figure 14). The unit thermo-economic cost of electricity in SA-CC-PG is smaller than in PG-CC and SA-PG-CC.

In contrast to solar-collector field investment, the unit cost of CO_2 in PG-CC is equal to that in SA-PG-CC, and is positively correlated with solar-collector field investment in SA-CC-PG (Figure 15).

In SA-CC-PG, the solar exergy and the corresponding thermo-economic cost are introduced in the CO_2 capture process so that the thermo-economic cost of electricity is not affected. In SA-PG-CC, the solar exergy and the thermo-economic cost flow into the power generation process; therefore, the unit cost of CO_2 remains constant and the thermo-economic cost of electricity changes. The solar-collector field investment assumes a significant proportion in the whole system and influences the thermo-economic cost of electricity greatly in SA-PG-CC and the unit cost of CO_2 in SA-CC-PG. To promote the exergy efficiency of solar field and reduce the investment, improving the design of the technology is necessary for the effective utilization of solar thermal energy.

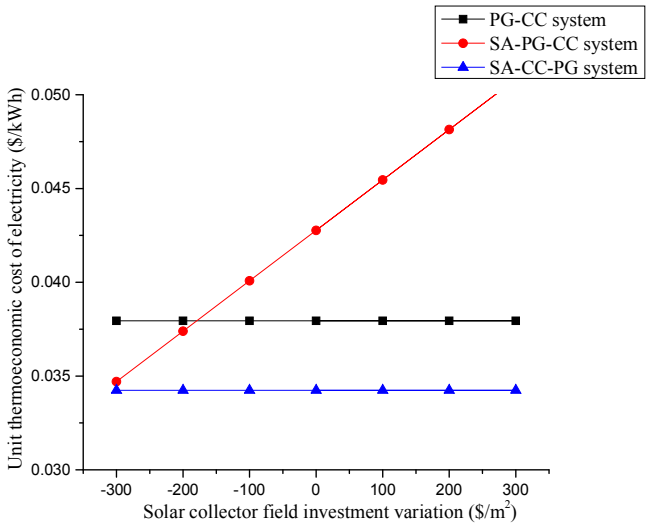

Figure 14. Variation in unit thermo-economic cost of electricity and solar-collector field investment for coal-fired power-generation system with MEA-based CO_2 capture (PG-CC), solar-aided coal-fired power generation with CO_2 capture (SA-PG-CC) and solar-aided CO_2 capture coal-fired power generation (SA-CC-PG).

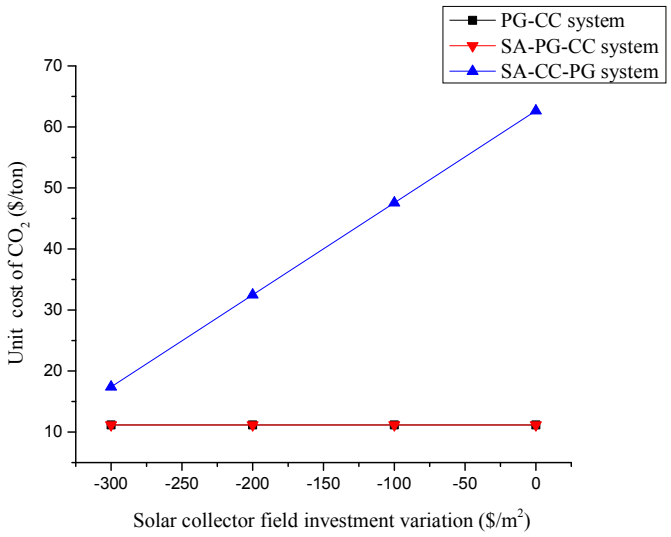

Figure 15. Variation in unit cost of CO_2 and solar-collector field investment for coal-fired power-generation system with MEA-based CO_2 capture (PG-CC), solar-aided coal-fired power generation with CO_2 capture (SA-PG-CC) and solar-aided CO_2 capture coal-fired power generation (SA-CC-PG).

5. Conclusions

In this paper, we analysed PG-CC, SA-PG-CC and SA-CC-PG systems based on the thermo-economics theory. Our conclusions are as follows:

1. Both SA-PG-CC and SA-CC-PG systems have greater power generation than the PG-CC system, and greater system efficiency. Compared with PG-CC, the coal consumption rate of SA-PG-CC and SA-CC-PG fell by 15.31 and 51.41 g/kWh, respectively. In this research, only the first high-pressure extraction steam was replaced by solar thermal. The other extraction steam can also be replaced with more solar thermal energy. The higher equivalent solar-power generation efficiency in SA-PG-CC indicates that the solar thermal energy is more fully used in SA-PG-CC system than in SA-CC-PG; therefore, the SA-PG-CC is a better configuration than SA-CC-PG.
2. In SA-PG-CC, the additional exergy cost of the solar-collector subsystem was distributed to other components in the power-generation process. Therefore, the unit exergy cost of each component increased slightly compared with PG-CC, and the unit exergy cost of the electricity increased by 13.2%. SA-CC-PG had a greater amount of power generation than PG-CC, and therefore slightly lower unit exergy costs of electricity and coal combustion rate in SA-CC-PG. However, the increased low-pressure steam also increased the exergy cost of other components. In SA-CC-PG, the heat required for the stripper reboiler is provided by solar thermal with higher exergy cost. Therefore, the unit exergy cost of CO_2 in SA-CC-PG was significantly greater than in PG-CC and SA-PG-CC.
3. Compared with PG-CC, the thermo-economic cost of electricity increased by 12.71% in SA-PG-CC and decreased by 9.77% in SA-CC-PG. The unit thermo-economic cost of CO_2 was much higher in SA-CC-PG because of the large thermo-economic cost of solar thermal energy.
4. The increased solar thermal energy improved the efficiency of the system in SA-PG-CC compared to PG-CC, indicating a high efficiency of solar exergy to electricity in this integration. The increased exergy cost shows the great exergy loss of the solar field. The increase of the unit thermo-economic cost of electricity indicates the enormous investment in solar fields. Therefore, to improve the thermo-economic performance of the solar energy system, the exergy efficiency of the solar field should be promoted and investment should be reduced.
5. Only two integration configurations are studied in this research, and there might be better methods for the integration of solar energy systems and CO_2 capture processes in coal-fired power plants. Using a general approach to optimize the solar thermal energy distribution in power generation and CO_2 capture process could be studied in future research.

Author Contributions: Rongrong Zhai conceived the models of related systems; Rongrong Zhai and Hongtao Liu calculated and analyzed financial data together; Rongrong Zhai, Hongtao Liu and Hao Wu wrote the manuscript, Rongrong Zhai, Hongtao Liu and Yongping Yang revised the manuscript; and Hai Yu helped in English modification. All authors agreed on the final version of the manuscript.

Funding: The research work is supported by the National Basic Research Program of China (No. 2015CB251505), China National Natural Science Foundation (No. 51106048), and the Fundamental Research Funds for the Central Universities and 111 Project (B12034).

Conflicts of Interest: The authors declare no conflict of interest.

Nomenclature

Symbol	Meaning	Unit
A	Total net aperture area of solar collector field	m^2
B	Exergy flow	kW
B^*	External exergy consumed for the product	kW
c_P	Unit thermo-economic cost	\$/kJ

Symbol	Meaning	Unit
c_{FB}	Thermo-economic cost of fuel	\$/kJ
c_I	Thermo-economic cost caused by irreversible	\$/kJ
c_N	Thermo-economic cost caused by negentropy	\$/kJ
c_Z	The thermo-economic cost caused by investment	\$/kJ
DNI	Solar direct normal irradiation	W/m^2
E_{coal}	Coal exergy	kW
F	Flue flow	kJ
P	Product flow	kJ
FB	Exergy fuel	kW
FS	Negentropy fuel	kW
k^*	Unit exergy cost	kW/kW
kB	Fuel exergy of unit of product	kW/kW
kI	Irreversible exergy lost of unit production	kW/kW
kS	Negentropy fuel of unit of product	kW/kW
KZ	Capital costs of unit production	\$/kJ
I	Irreversible exergy loss of production	kW/kW
Z	Non-energy costs of the component	\$
c_F	Energy costs of the component	\$/kJ
i	Component number of input flow	-
j	Component number of output flow	-
$\eta_{removal}$	CO_2 removal ratio	–
η_{load}	CO_2 loading ratio	–

Appendix A

Table A1. Abbreviations and Components.

ID	Abbreviation	Component
1–4,6–8	FWH	Feed-water heater
8	OWHE	Oil–water heat exchanger
5	DTR	Deaerator
9	SH	Boiler superheater
10	RH	Reheater
11,12	HP	High-pressure turbine
13,14	IP	Intermediate-pressure turbine
15–19	LP	Low-pressure turbine
20	BFPT	Feed-water pump turbine
21	FWP	Feed-water pump
22	CP	Condenser water pump
23	CND	Condenser
24	GEN	Generator
25	COL	Collector
26	COLP	Collector oil-pump
27	CCS	MEA-based CO_2 capture subsystem

Appendix B

Table A2. Investment of Each Component [48,66].

ID	Component	PG-CC ($)	SA-PG-CC ($)	SA-CC-PG ($)
1	FWH7	1,871,692	1,871,692	1,855,075
2	FWH6	884,416	884,416	876,554
3	FWH5	934,189	934,189	925,895
4	FWH4	862,262	862,262	854,604
5	DTR	1,886,061	1,886,061	1,886,061
6	FWH3	1,752,092	1,735,706	1,485,249
7	FWH2	2,649,115	2,637,052	2,245,656
8	FWH1/OWHE	2,427,635	2,456,082	2,057,915
9	SH	224,373,329	220,422,356	223,888,459
10	RH	52,032,176	55,983,149	52,517,046
11	HP1	20,010,303	17,572,405	16,317,348
12	HP2	8,301,811	7,979,165	6,769,733
13	IP1	11,829,994	11,362,524	9,646,736
14	IP2	11,629,111	11,169,992	9,482,927
15	LP1	7,420,385	7,142,714	6,050,932
16	LP2	6,633,423	6,386,493	5,409,206
17	LP3	4,200,176	4,218,248	5,598,987
18	LP4	2,408,251	2,578,164	4,951,836
19	LP5	4,309,719	4,756,450	10,433,958
20	BFPT	3,902,195	3,902,195	3,902,195
21	FWP	7,641,799	7,641,799	7,641,799
22	CP	357,701	357,701	357,701
23	CND	29,835,535	29,835,535	29,835,535
24	GEN	40,647,868	40,647,868	40,647,868
25	COL	-	191,624,287	862,309,293
26	COLP	-	6401	6401
27	CCS	186,025,000	186,025,000	186,025,000

Appendix C

Table A3. Investment of Each Component in the MEA-Based CO_2 Capture Subsystem [67–69].

Component	500-MW CO_2 Capture System ($)	1000-MW CO_2 Capture System ($)
Flue gas blower	2,172,000	3,291,000
Absorber	30,690,000	46,516,000
Rich solution pump	4,480,000	6,789,000
Lean/rich solution heat exchanger	2,175,000	3,295,000
Lean solution cooler	3,684,000	5,583,000
Stripper	16,410,000	24,873,000
Reboiler	10,180,000	15,429,000
Circulating water pump	3,684,000	5,583,000
Drying and compression device	32,217,616	54,128,000
MEA solution	13,850,000	17,113,000
Corrosion inhibitor	2,771,000	3,425,000

Appendix D

Table A4. Results of Exergy Cost (kW/kW) in the PG-CC, SA-PG-CC and SA-CC-PG Systems.

ID	Component	PG-CC				SA-PG-CC				SA-CC-PG			
		k_P^*	k_{FB}^*	k_I^*	k_N^*	k_P^*	k_{FB}^*	k_I^*	k_N^*	k_P^*	k_{FB}^*	k_I^*	k_N^*
1	FWH7	2.62	1.91	0.62	0.09	2.99	2.18	0.71	0.10	2.64	1.93	0.63	0.08
2	FWH6	2.17	1.91	0.23	0.03	2.48	2.18	0.26	0.04	2.19	1.93	0.23	0.03
3	FWH5	2.16	1.91	0.22	0.03	2.47	2.18	0.25	0.03	2.18	1.93	0.22	0.03
4	FWH4	2.14	1.91	0.21	0.03	2.45	2.18	0.23	0.03	2.16	1.93	0.21	0.03
5	DTR	2.13	1.91	0.19	0.03	2.44	2.18	0.22	0.03	2.15	1.93	0.19	0.03
6	FWH3	2.12	1.91	0.19	0.03	2.44	2.18	0.23	0.03	2.15	1.93	0.19	0.03
7	FWH2	2.03	1.91	0.10	0.01	2.33	2.18	0.13	0.02	2.05	1.93	0.11	0.01
8	FWH1/OWHE	2.02	1.91	0.10	0.01	6.67	5.84	0.53	0.30	2.05	1.93	0.10	0.01
9	SH	1.85	1.00	0.67	0.18	1.87	1.00	0.67	0.20	1.85	1.00	0.68	0.18
10	RH	1.84	1.00	0.67	0.17	1.86	1.00	0.67	0.20	1.92	1.00	0.76	0.17
11	HP1	2.07	1.91	0.14	0.02	2.37	2.18	0.16	0.02	2.10	1.93	0.15	0.02
12	HP2	2.05	1.91	0.12	0.02	2.29	2.18	0.09	0.02	2.07	1.93	0.12	0.02
13	IP1	2.63	1.91	0.71	0.01	2.28	2.18	0.08	0.01	2.01	1.93	0.07	0.01
14	IP2	1.99	1.91	0.07	0.01	2.27	2.18	0.08	0.01	2.02	1.93	0.08	0.01
15	LP1	1.99	1.91	0.07	0.01	2.27	2.18	0.08	0.01	2.01	1.93	0.07	0.01
16	LP2	1.99	1.91	0.07	0.01	2.28	2.18	0.08	0.01	2.01	1.93	0.07	0.01
17	LP3	1.99	1.91	0.07	0.01	2.29	2.18	0.09	0.01	2.02	1.93	0.08	0.01
18	LP4	2.01	1.91	0.09	0.01	2.30	2.18	0.10	0.01	2.03	1.93	0.09	0.01
19	LP5	2.09	1.91	0.16	0.02	2.39	2.18	0.18	0.02	2.11	1.93	0.16	0.02
20	BFPT	2.37	1.91	0.40	0.06	2.71	2.18	0.46	0.06	2.39	1.93	0.41	0.05
21	FWP	2.66	2.37	0.26	0.03	3.12	2.75	0.33	0.04	2.68	2.39	0.26	0.03
22	CP	3.05	2.43	0.55	0.06	3.22	2.75	0.39	0.07	2.61	2.08	0.47	0.06
23	CND	4.89	1.91	2.97	0.00	5.52	2.18	3.33	0.00	4.70	1.93	2.77	0.00
24	GEN	2.43	2.40	0.03	0.00	2.75	2.72	0.03	0.00	2.08	2.05	0.02	0.00
25	COL	-	-	-	-	5.84	1.00	4.84	0.00	7.35	1.00	6.35	0.00
26	COLP	-	-	-	-	4.74	2.75	2.11	0.00	3.22	2.75	0.46	0.00

Appendix E

Table A5. Results of Thermo-Economic Cost ($/kJ) in the PG-CC, SA-PG-CC and SA-CC-PG Systems.

		PG-CC					SA-PG-CC					SA-CC-PG				
ID	**Component**	c_P	c_{FB}	c_I	c_N	c_Z	c_P	c_{FB}	c_I	c_N	c_Z	c_P	c_{FB}	c_I	c_N	c_Z
1	FWH7	14.64	7.84	2.54	3.21	1.05	14.41	9.65	3.13	0.66	0.98	11.48	7.54	2.44	0.46	1.04
2	FWH6	10.70	7.84	0.94	1.19	0.72	11.72	9.65	1.16	0.24	0.67	9.33	7.54	0.91	0.17	0.71
3	FWH5	10.47	7.84	0.89	1.12	0.61	11.54	9.65	1.09	0.23	0.57	9.17	7.54	0.85	0.17	0.61
4	FWH4	10.29	7.84	0.84	1.06	0.54	11.41	9.65	1.04	0.22	0.51	9.04	7.54	0.81	0.15	0.54
5	DTR	10.48	7.84	0.79	0.99	0.85	11.64	9.65	0.99	0.21	0.79	9.29	7.54	0.76	0.14	0.85
6	FWH3	10.10	7.84	0.77	0.97	0.52	11.39	9.65	1.01	0.21	0.52	8.86	7.54	0.74	0.15	0.43
7	FWH2	9.29	7.84	0.43	0.54	0.47	10.79	9.65	0.55	0.12	0.48	8.43	7.54	0.41	0.08	0.40
8	FWH1/OWHE	9.21	7.84	0.41	0.52	0.44	36.83	31.51	2.88	2.00	0.44	8.38	7.54	0.40	0.08	0.36
9	SH	12.72	2.00	1.33	6.68	2.71	7.41	2.00	1.34	1.37	2.70	7.02	2.00	1.36	0.97	2.69
10	RH	12.44	2.00	1.33	6.39	2.71	7.35	2.00	1.34	1.31	2.70	7.16	2.00	1.51	0.93	2.72
11	HP1	10.24	7.84	0.58	0.73	1.08	11.49	9.65	0.73	0.15	0.97	9.10	7.54	0.57	0.11	0.88
12	HP2	10.03	7.84	0.50	0.61	1.08	11.11	9.65	0.38	0.12	0.97	8.99	7.54	0.48	0.09	0.88
13	IP1	12.18	7.84	2.90	0.35	1.08	11.05	9.65	0.37	0.07	0.97	8.76	7.54	0.29	0.05	0.88
14	IP2	9.54	7.84	0.28	0.34	1.08	11.02	9.65	0.34	0.07	0.97	8.78	7.54	0.30	0.06	0.88
15	LP1	9.52	7.84	0.28	0.32	1.08	11.02	9.65	0.34	0.07	0.97	8.74	7.54	0.27	0.05	0.88
16	LP2	9.59	7.84	0.30	0.36	1.08	11.06	9.65	0.37	0.07	0.97	8.77	7.54	0.29	0.05	0.89
17	LP3	9.61	7.84	0.30	0.38	1.08	11.10	9.65	0.41	0.08	0.97	8.80	7.54	0.32	0.06	0.88
18	LP4	9.70	7.84	0.35	0.42	1.08	11.14	9.65	0.44	0.09	0.97	8.82	7.54	0.34	0.06	0.88
19	LP5	10.37	7.84	0.64	0.80	1.08	11.57	9.65	0.79	0.16	0.97	9.16	7.54	0.62	0.12	0.88
20	BFPT	13.22	7.84	1.65	2.07	1.66	13.76	9.65	2.03	0.42	1.66	11.08	7.54	1.59	0.30	1.65
21	FWP	17.50	11.55	1.28	1.07	3.60	18.36	13.76	1.66	0.24	2.71	16.05	11.08	1.22	0.15	3.60
22	CP	21.85	10.54	2.37	2.39	6.56	20.16	11.88	1.68	0.49	6.12	18.56	9.51	2.14	0.35	6.56
23	CND	34.60	7.84	12.30	0.00	14.46	36.92	9.65	24.01	0.00	12.59	25.63	7.54	18.32	0.00	7.15
24	GEN	10.54	9.83	0.12	0.00	0.58	11.88	11.20	0.13	0.00	0.54	9.51	8.92	0.11	0.00	0.48
25	COL	-	-	-	-	-	31.51	0.00	0.00	0.00	31.51	39.70	0.00	0.00	0.00	39.70
26	COLP	-	-	-	-	-	22.08	11.88	8.58	0.00	1.62	14.71	11.88	1.99	0.00	0.84

References

1. Rogelj, J.; den Elzen, M.; Hohne, N.; Fransen, T.; Fekete, H.; Winkler, H.; Schaeffer, R.; Sha, F.; Riahi, K.; Meinshausen, M. Paris Agreement climate proposals need a boost to keep warming well below 2 degrees C. *Nature* **2016**, *534*, 631–639. [CrossRef] [PubMed]
2. International Energy Agency (IEA). *World Energy Outlook 2017*; Organisation for Economic Co-operation and Development: Paris, France, 2017.
3. International Energy Agency (IEA). *Key World Energy Statistics*; International Energy Agency: Paris, France, 2017.
4. Karimi, F.; Khalilpour, R. Evolution of carbon capture and storage research: Trends of international collaborations and knowledge maps. *Int. J. Greenh. Gas Control* **2015**, *37*, 362–376.
5. Li, K.; Yu, H.; Yan, S.; Feron, P.; Wardhaugh, L.; Tade, M. Technoeconomic Assessment of an Advanced Aqueous Ammonia-Based Postcombustion Capture Process Integrated with a 650-MW Coal-Fired Power Station. *Environ. Sci. Technol.* **2016**, *50*, 10746–10755. [CrossRef] [PubMed]
6. Mumford, A.; Wu, Y.; Smith, H.; Geoffrey, S. Review of solvent based carbon-dioxide capture technologies. *Front. Chem. Sci. Eng.* **2015**, *9*, 125–141. [CrossRef]
7. Zhao, S.; Feron, P.H.M.; Deng, L.; Favre, E.; Chabanon, E.; Yan, S.; Hou, J.; Chen, V.; Qi, H. Status and progress of membrane contactors in post-combustion carbon capture: A state-of-the-art review of new developments. *J. Membr. Sci.* **2016**, *511*, 180–206. [CrossRef]
8. Theo, W.L.; Lim, J.S.; Hashim, H.; Mustaffa, A.A.; Ho, W.S. Review of pre-combustion capture and ionic liquid in carbon capture and storage. *Appl. Energy* **2016**, *183*, 1633–1663. [CrossRef]
9. Li, K.; Leigh, W.; Feron, P.; Yu, H.; Tade, M. Systematic study of aqueous monoethanolamine (MEA)-based CO_2 capture process: Techno-economic assessment of the MEA process and its improvements. *Appl. Energy* **2016**, *165*, 648–659. [CrossRef]
10. Oh, S.-Y.; Binns, M.; Cho, H.; Kim, J.-K. Energy minimization of MEA-based CO_2 capture process. *Appl. Energy* **2016**, *169*, 353–362. [CrossRef]
11. Zhang, W.; Liu, H.; Sun, Y.; Cakstins, J.; Sun, C.; Snape, C.E. Parametric study on the regeneration heat requirement of an amine-based solid adsorbent process for post-combustion carbon capture. *Appl. Energy* **2016**, *168*, 394–405. [CrossRef]
12. Final Report for the Project 'Development of an Aqueous Ammonia-Based PCC Technology for Australian Conditions'. Available online: http://anlecrd.com.au/wp-content/uploads/2016/08/Aqueous-Ammonia-Final-Report.pdf (accessed on 9 October 2017).
13. CO_2 Capture Technologies—Post Combustion Capture (PCC). Available online: http://www.globalccsinstitute.com/publications/CO2-capture-technologies-post-combustion-capture-pcc (accessed on 9 October 2017).
14. Petra Nova Carbon Capture. Available online: https://www.globalccsinstitute.com/projects/petra-nova-carbon-capture-project (accessed on 24 July 2017).
15. Lemaire, E.; Bouillon, P.A.; Lettat, K. Development of HiCapt+ TM Process for CO_2 Capture from Lab to Industrial Pilot Plant. *Oil Gas Sci. Technol. Rev. IFP Energies Nouv.* **2014**, *69*, 1069–1080. [CrossRef]
16. Li, K.; Cousins, A.; Yu, H.; Feron, P.; Tade, M.; Luo, W.; Chen, J. Systematic study of aqueous monoethanolamine-based CO_2capture process: Model development and process improvement. *Energy Sci. Eng.* **2016**, *4*, 23–39. [CrossRef]
17. Øi, L.E.; Bråthen, T.; Berg, C.; Brekne, S.K.; Flatin, M.; Johnsen, R.; Moen, I.G.; Thomassen, E. Optimization of Configurations for Amine based CO_2 Absorption Using Aspen HYSYS. *Energy Procedia* **2014**, *51*, 224–233. [CrossRef]
18. Chen, E.; Zhang, Y.; Sachde, D.; Lin, Y.J.; Rochelle, G.T. Evaluated Pilot Plant Results for 5 m Piperazine with the Advanced Flash Stripper. 2015. Available online: http://ieaghg.org/docs/General_Docs/PCCC3_PDF/5_PCCC3_6_Chen.pdf (accessed on 9 October 2017).
19. Jiang, K.; Li, K.; Yu, H.; Chen, Z.; Wardhaugh, L.; Feron, P. Advancement of ammonia based post-combustion CO_2 capture using the advanced flash stripper process. *Appl. Energy* **2017**, *202*, 496–506. [CrossRef]
20. Zhang, Y.; Ji, X.; Xie, Y.; Lu, X. Screening of conventional ionic liquids for carbon dioxide capture and separation. *Appl. Energy* **2016**, *162*, 1160–1170. [CrossRef]
21. Kunze, A.-K.; Dojchinov, G.; Haritos, V.S.; Lutze, P. Reactive absorption of CO_2 into enzyme accelerated solvents: From laboratory to pilot scale. *Appl. Energy* **2015**, *156*, 676–685. [CrossRef]
22. Wang, X.; Akhmedov, N.G.; Hopkinson, D.; Hoffman, J.; Duan, Y.; Egbebi, A.; Resnik, K.; Li, B. Phase change amino acid salt separates into CO_2-rich and CO_2-lean phases upon interacting with CO_2. *Appl. Energy* **2016**, *161*, 41–47. [CrossRef]

23. Le Moullec, Y.; Kanniche, M. Screening of flowsheet modifications for an efficient monoethanolamine (MEA) based post-combustion CO_2 capture. *Int. J. Greenh. Gas Control* **2011**, *5*, 727–740. [CrossRef]
24. Ahn, H.; Luberti, M.; Liu, Z.; Brandani, S. Process configuration studies of the amine capture process for coal-fired power plants. *Int. J. Greenh. Gas Control* **2013**, *16*, 29–40. [CrossRef]
25. Cousins, A.; Wardhaugh, L.T.; Feron, P.H.M. Preliminary analysis of process flow sheet modifications for energy efficient CO_2 capture from flue gases using chemical absorption. *Chem. Eng. Res. Des.* **2011**, *89*, 1237–1251. [CrossRef]
26. Cousins, A.; Wardhaugh, L.T.; Feron, P.H.M. A survey of process flow sheet modifications for energy efficient CO_2 capture from flue gases using chemical absorption. *Int. J. Greenh. Gas Control* **2011**, *5*, 605–619. [CrossRef]
27. Bui, M.; Gunawan, I.; Verheyen, V.; Feron, P.; Meuleman, E.; Adeloju, S. Dynamic modelling and optimisation of flexible operation in post-combustion CO_2 capture plants—A review. *Comput. Chem. Eng.* **2014**, *61*, 245–265. [CrossRef]
28. Bui, M.; Fajardy, M.; Mac Dowell, N. Bio-Energy with CCS (BECCS) performance evaluation: Efficiency enhancement and emissions reduction. *Appl. Energy* **2017**, *195*, 289–302. [CrossRef]
29. Harkin, T.; Hoadley, A.; Hooper, B. Process integration analysis of a brown coal-fired power station with CO_2 capture and storage and lignite drying. *Energy Procedia* **2009**, *1*, 3817–3825. [CrossRef]
30. Harkin, T.; Hoadley, A.; Hooper, B. Reducing the energy penalty of CO_2 capture and compression using pinch analysis. *J. Clean. Prod.* **2010**, *18*, 857–866. [CrossRef]
31. Xu, G.; Hu, Y.; Tang, B.; Yang, Y.; Zhang, K.; Liu, W. Integration of the steam cycle and CO_2 capture process in a decarbonization power plant. *Appl. Therm. Eng.* **2014**, *73*, 277–286. [CrossRef]
32. Xu, G.; Huang, S.; Yang, Y.; Wu, Y.; Zhang, K.; Xu, C. Techno-economic analysis and optimization of the heat recovery of utility boiler flue gas. *Appl. Energy* **2013**, *112*, 907–917. [CrossRef]
33. Hu, Y.; Xu, G.; Xu, C.; Yang, Y. Thermodynamic analysis and techno-economic evaluation of an integrated natural gas combined cycle (NGCC) power plant with post-combustion CO_2 capture. *Appl. Therm. Eng.* **2017**, *111*, 308–316. [CrossRef]
34. Pfaff, I.; Oexmann, J.; Kather, A. Optimised integration of post-combustion CO_2 capture process in greenfield power plants. *Energy* **2010**, *35*, 4030–4041. [CrossRef]
35. Liu, X.; Chen, J.; Luo, X.; Wang, M.; Meng, H. Study on heat integration of supercritical coal-fired power plant with post-combustion CO_2 capture process through process simulation. *Fuel* **2015**, *158*, 625–633. [CrossRef]
36. Wang, D.; Bao, A.; Kunc, W.; Liss, W. Coal power plant flue gas waste heat and water recovery. *Appl. Energy* **2012**, *91*, 341–348. [CrossRef]
37. Bui, M.; Fajardy, M.; Mac Dowell, N. Bio-energy with carbon capture and storage (BECCS): Opportunities for performance improvement. *Fuel* **2018**, *213*, 164–175. [CrossRef]
38. Mokhtar, M.; Ali, M.T.; Khalilpour, R.; Abbas, A.; Shah, N.; Hajaj, A.A.; Armstrong, P.; Chiesa, M.; Sgouridis, S. Solar-assisted Post-combustion Carbon Capture feasibility study. *Appl. Energy* **2012**, *92*, 668–676. [CrossRef]
39. Zhao, Y.; Hong, H.; Zhang, X.; Jin, H. Integrating mid-temperature solar heat and post-combustion CO_2-capture in a coal-fired power plant. *Sol. Energy* **2012**, *86*, 3196–3204. [CrossRef]
40. Zhai, R.; Qi, J.; Zhu, Y.; Zhao, M.; Yang, Y. Novel system integrations of 1000 MW coal-fired power plant retrofitted with solar energy and CO_2 capture system. *Appl. Therm. Eng.* **2017**, *125*, 1133–1145. [CrossRef]
41. Wang, J.; Zhao, J.; Wang, Y.; Deng, S.; Sun, T.; Li, K. Application potential of solar-assisted post-combustion carbon capture and storage (CCS) in China: A life cycle approach. *J. Clean. Prod.* **2017**, *154*, 541–552. [CrossRef]
42. Wang, F.; Zhao, J.; Li, H.; Deng, S.; Yan, J. Preliminary experimental study of post-combustion carbon capture integrated with solar thermal collectors. *Appl. Energy* **2017**, *185*, 1471–1480. [CrossRef]
43. Rezazadeh, F.; Gale, W.F.; Lin, Y.-J.; Rochelle, G.T. Energy Performance of Advanced Reboiled and Flash Stripper Configurations for CO_2 Capture Using Monoethanolamine. *Ind. Eng. Chem. Res.* **2016**, *55*, 4622–4631. [CrossRef]
44. Liu, L.; Zhao, J.; Deng, S.; An, Q. A technical and economic study on solar-assisted ammonia-based post-combustion CO_2 capture of power plant. *Appl. Therm. Eng.* **2016**, *102*, 412–422. [CrossRef]
45. Lassagne, O.; Iliuta, M.C.; Gosselin, L.; Désilets, M. Techno-economic assessment of CO_2capture from aluminum smelter emissions using PZ activated AMP solutions. *Can. J. Chem. Eng.* **2016**, *94*, 761–770. [CrossRef]
46. Raksajati, A.; Ho, M.T.; Wiley, D.E. Techno-economic Evaluation of CO_2 Capture from Flue Gases Using Encapsulated Solvent. *Ind. Eng. Chem. Res.* **2017**, *56*, 1604–1620. [CrossRef]

47. Gao, J.; Yin, J.; Zhu, F.; Chen, X.; Tong, M.; Kang, W.; Zhou, Y.; Lu, J. Environmental Effects Comparison of absorption and regeneration performance for post-combustion CO_2 capture by mixed MEA solvents. *Energy Sources Part A* **2016**, *38*, 2530–2535. [CrossRef]
48. Zhai, R.; Liu, H.; Li, C.; Zhao, M.; Yang, Y. Analysis of a solar-aided coal-fired power generation system based on thermo-economic structural theory. *Energy* **2016**, *102*, 375–387. [CrossRef]
49. Lozano, M.A.; Valero, A. Theory of the exergetic cost. *Energy* **1993**, *18*, 939–960. [CrossRef]
50. Chao, Z. Thermoeconomic Analysis and Optimization of Complex Energy Systems. Ph.D. Thesis, Huazhong University of Science and Technology, Wuhan, China, 2006. (In Chinese)
51. Tsatsaronis, G. Thermoeconomic analysis and optimization of energy systems. *Prog. Energy Combust. Sci.* **1993**, *19*, 227–257. [CrossRef]
52. Booras, G.; Davison, J.; Ekstrom, C.; Matuszewski, M.; Short, C. *Toward a Common Method of Cost Estimation for CO_2 Capture and Storage at Fossil Fuel Power Plants*; Global CCS Institute: Docklands, Australia, 2013.
53. Ehlers, S.; Roeder, V.; Liebenthal, U.; Kather, I.A. *Techno Economic Evaluation Different Post Combustion CO_2 Capture Process Flow Sheet*; Hamburg University of Technology: Hamburg, Germany, 2014.
54. Valero, A.; Serra, L.; Uche, J. Fundamentals of Exergy Cost Accounting and Thermoeconomics. Part II: Applications. *J. Energy Resour. Technol.* **2006**, *128*, 9–15. [CrossRef]
55. Han, Y.; Xu, G.; Zheng, Q.; Xu, C.; Hu, Y.; Yang, Y.; Lei, J. New heat integration system with bypass flue based on the rational utilization of low-grade extraction steam in a coal-fired power plant. *Appl. Therm. Eng.* **2017**, *113*, 460–471. [CrossRef]
56. Wang, L.; Yang, Y.; Dong, C.; Morosuk, T.; Tsatsaronis, G. Multi-objective optimization of coal-fired power plants using differential evolution. *Appl. Energy* **2014**, *115*, 254–264. [CrossRef]
57. Gewald, D.; Karellas, S.; Schuster, A.; Spliethoff, H. Integrated system approach for increase of engine combined cycle efficiency. *Energy Convers. Manag.* **2012**, *60*, 36–44. [CrossRef]
58. Burin, E.K.; Vogel, T.; Multhaupt, S.; Thelen, A.; Oeljeklaus, G.; Görner, K.; Bazzo, E. Thermodynamic and economic evaluation of a solar aided sugarcane bagasse cogeneration power plant. *Energy* **2016**, *117*, 416–428. [CrossRef]
59. Al-Maliki, W.A.K.; Alobaid, F.; Kez, V.; Epple, B. Modelling and dynamic simulation of a parabolic trough power plant. *J. Process Control* **2016**, *39*, 123–138. [CrossRef]
60. Krüger, M.; Bartsch, P.; Pointner, H.; Zunft, S. Solar tower power plant using a particle-heated steam generator: Modeling and parametric study. In *AIP Conference Proceedings*; AIP Publishing: Melville, NY, USA, 2016; Volume 1734, p. 050025.
61. Pei, X.; He, B.; Yan, L.; Wang, C.; Song, W.; Song, J. Process simulation of oxy-fuel combustion for a 300 MW pulverized coal-fired power plant using Aspen Plus. *Energy Convers. Manag.* **2013**, *76*, 581–587. [CrossRef]
62. Li, K.; Yu, H.; Feron, P.; Wardhaugh, L.; Tade, M. Techno-economic assessment of stripping modifications in an ammonia-based post-combustion capture process. *Int. J. Greenh. Gas Control* **2016**, *53*, 319–327. [CrossRef]
63. Rezazadeh, F.; Gale, W.F.; Akram, M.; Hughes, K.J.; Pourkashanian, M. Performance evaluation and optimisation of post combustion CO_2 capture processes for natural gas applications at pilot scale via a verified rate-based model. *Int. J. Greenh. Gas Control* **2016**, *53*, 243–253. [CrossRef]
64. Baghernejad, A.; Yaghoubi, M. Exergoeconomic analysis and optimization of an Integrated Solar Combined Cycle System (ISCCS) using genetic algorithm. *Energy Convers. Manag.* **2011**, *52*, 2193–2203. [CrossRef]
65. Miao, Z. *Research on Performance of Carbon Capture System for Solar-Added Coal Fired Power Generation*; North China Electric Power University: Beijing, China, 2016.
66. Electric Power Planning & Engineering Institute. *The Reference Cost Index of Thermal Power Engineering Rationed Design*; China Electric Power Press: Beijing, China, 2012; pp. 257–331.
67. Xiong, J. *Thermo-Economic Cost Analysis and Optimization of Conventional Coal-Fired Power Generation System and CO_2 Capture System*; Huazhong University of Science and Technology: Wuhan, China, 2007.
68. Rao, A. *A Technical, Environmental, and Economic Assessment of Amine-Based Carbon Capture Technologies for Greenhouse Gas Control*; Department of Engineering and Public Policy: Washington, DC, USA, 2003.
69. Hong, H.; Peng, S.; Zhao, Y.; Liu, Q.; Jin, H. A Typical Solar-coal Hybrid Power Plant in China. *Energy Procedia* **2014**, *49*, 1777–1783. [CrossRef]

© 2018 by the authors. Licensee MDPI, Basel, Switzerland. This article is an open access article distributed under the terms and conditions of the Creative Commons Attribution (CC BY) license (http://creativecommons.org/licenses/by/4.0/).